

Copyright

by

Kiran Mallavarapu

2001

**Feedback Control
of Ionic Polymer Actuators**

by

Kiran Mallavarapu

Thesis submitted to the Faculty of the
Virginia Polytechnic Institute and State University
in partial fulfillment of the requirements for the degree of

Master of Science

in

Mechanical Engineering

Donald J. Leo, Chair
Daniel J. Inman
Ronald G. Kander

July 2001

Blacksburg, Virginia

To my father,
M. Adinarayana Murthy,
and my mother,
P. Vijayalakshmi

Feedback Control of Ionic Polymer Actuators

Kiran Mallavarapu, M.S.

Virginia Polytechnic Institute and State University, 2001

Advisor: Donald J. Leo

ABSTRACT

An ionic polymer actuator consists of a thin Nafion-117 sheet plated with gold or platinum on both sides. An ionic polymer actuator undergoes large deformation in the presence of low applied voltage across its thickness and exhibits low impedance. They can also be used as large displacement sensors by bending them to induce stresses and generate a voltage response. They operate best in a humid environment. Ionic polymer actuators have been used for various practical applications such as bio-mimetic robotic propulsion, flexible low mass robotic arms, propellers for swimming robotic structures, linear and platform type robotic actuators and active catheter systems.

One of the disadvantages of ionic polymer actuators is that their settling time to a unit step voltage is on the order of 5-20 seconds in a cantilever configuration. The slow time constant of an ionic polymer limits the actuation bandwidth. The characteristics of ionic polymer actuators, low force and large displacement (as compared to other actuator technologies such as PZT or PVDF), cannot be used in applications requiring a faster response time for a given actuation signal. Due to this limitation, many applications will not be able to make use of the large displacement effectively because of the limited bandwidth of the actuator.

Another disadvantage of using an ionic polymer actuator is that the stiffness of the actuator is a function of the hydration of the polymer. Difficulties in controlling the hydration, which changes with respect to time, results in inconsistencies in the mechanical response exhibited by the polymers during continual usage.

Several physical models of ionic polymer actuators have been proposed. The physical phenomenon responsible for the bending is not completely understood and no clear set of principles have been able to explain the motion of the polymers completely. Physical phenomena like ionic motion, back diffusion of water and electrostatic force have been used to explain these models.

This research demonstrates the use of feedback control to overcome the limitation of slow settling time. First, an empirical model of the ionic polymers developed by Kanno was modified by studying the step response of these actuators. The empirical model is used to design a feedback compensator by state space modeling techniques. Since the ionic polymer actuator has a slow settling time in the open-loop, the design objectives are to minimize the settling time and constrain the control voltage to be less than a prescribed value. The controller is designed using Linear Quadratic Regulator (LQR) techniques which reduced the number of design parameters to one variable.

Simulations are performed which show settling times of 0.03 seconds for closed-loop feedback control are possible as compared to the open-loop settling time of 16-18 seconds. The maximum control voltage varied from 1.2 Volts to 3.5 Volts depending on the LQR design parameter. The controller is implemented and results obtained are consistent with the simulations. Closed-loop settling time is observed to be 4-8 seconds and the ratio of the peak response to the steady-state response is reduced by an order of magnitude.

Discrepancies between the experiment and the simulations are attributed to the inconsistencies in the resonant frequency of the actuator. Experiments demonstrate that changes in the surface hydration of the polymer result in 20% variations in the actuator resonance. Variations in the actuator resonance require a more conservative compensator design, thus limiting the performance of the feedback control system.

**Feedback Control
of Ionic Polymer Actuators**

**Approved by
Advising Committee:**

Acknowledgments

First, I must thank my advisor, Dr. Donald J. Leo, for his guidance and patience throughout my graduate studies. His support made my work and learning experience, a very special one. Also, I want to extend my thanks to Dr. Daniel J. Inman and Dr. Ron Kander for their support and enthusiasm as members of my advisory committee.

I am immensely grateful to my parents and my sister for the encouragement and support they have given me during my studies. They have endured many sacrifices to provide for my education. I promise to give them back my support all their lives. I must also thank Vasanthi for all her support during these years. Her love and attitude towards life have always motivated me to go on. I shall try to match her strong demonstration of love.

In addition, I want to thank my “teammates”. Thanks to Kenn Newbury for his invaluable suggestions and help during this entire research. I would also like to thank my other teammates Orion Parott and Matt Bennett for the discussions and ideas we exchanged and helping me with their experimental skills. Their suggestions, help, friendship and time was invaluable in assisting my research.

I also want to thank my colleagues in the Center for Intelligent Material Systems and Structures (CIMSS). Special thanks to Greg Pettit and Kevin Fahrenholt for their encouragement and many a helpful discussions, which have found their way into this research. The cooperation and good humor of everybody made it an unforgettable and enjoyable experience.

This work is supported by the Air Force Research Lab through a subcontract from University Space Research Association of Albuquerque, NM, contract number F29601-98-D-0210. I gratefully acknowledge the support. I would like to thank Dr. Mohsen Shahinpoor and Dr. Kwang Kim of the Mechanical Engineering Department of the University of New

Mexico for providing the polymer samples used in this project.

KIRAN MALLAVARAPU

Virginia Polytechnic Institute and State University

July 2001

Contents

Abstract	iv
Acknowledgments	vii
List of Tables	xii
List of Figures	xiii
Chapter 1 Introduction	1
1.1 Ionic Polymer Actuators	1
1.1.1 Comparison with other Actuator Technologies	2
1.2 Motivation	3
1.3 Literature Review and Background	4
1.3.1 Modeling	4
1.3.2 Summary	6
1.3.3 Preparation	7
1.3.4 Applications	10
1.4 Overview of Thesis	11
1.4.1 Research Objectives	11
1.4.2 Contribution	12
1.4.3 Approach	12
Chapter 2 Dynamic Response of Ionic Polymer Actuators	14
2.1 Previous Work	14
2.2 Step Voltage response	15
2.2.1 Test Setup	15

2.2.2	Experimental Results	16
2.3	Transfer functions	17
2.3.1	Test Setup	17
2.3.2	Experimental Results	18
2.4	Summary	21
Chapter 3 Empirical Modeling		22
3.1	Introduction	22
3.2	Empirical model by Kanno et al. (1994)	23
3.3	Modification of the Empirical Model	24
3.3.1	Optimization function: FMINCON	25
3.3.2	Test Setup	26
3.3.3	Optimized Results	27
3.4	Cost Function Analysis	29
3.4.1	Short Polymer	30
3.4.2	Long Polymer	31
3.4.3	Conclusions about the Cost Analysis	33
3.5	Summary	35
Chapter 4 Feedback Control		36
4.1	State Space Model	36
4.2	Design of Controller	39
4.2.1	Linear Quadratic Regulator(LQR) Control	39
4.2.2	Linear Observer-Estimator	40
4.3	Closed-loop Control Simulation	42
4.3.1	Short polymer	42
4.3.2	Case 1: Long polymer - Resonance term included in Q	47
4.3.3	Case 2: Long Polymer - Resonance term ignored in Q	51
4.3.4	Simulations with Perturbation	55
4.4	Summary	60
Chapter 5 Experimental Analysis		61
5.1	Experimental setup	61

5.2	Experimental Results	63
5.2.1	Short Polymer	63
5.2.2	Long Polymer	66
5.2.3	Analysis of Results	69
5.3	Summary	71
Chapter 6 Contributions, Conclusions, Recommendations and Future Work		72
6.1	Contributions	72
6.2	Conclusions	73
6.3	Recommendations and Future Work	75
Bibliography		77
Vita		81

List of Tables

1.1	Comparison of Actuator Technologies	3
2.1	Actuator Samples and their Sizes	16
3.1	Empirical model for short polymer using 2 real poles and one resonance term	30
3.2	Empirical model for short polymer using 3 real poles and one resonance term	30
3.3	Empirical model for short polymer using 4 real poles and one resonance term	31
3.4	Average cost function as number of real poles vary for short polymer	31
3.5	Empirical model for long polymer using 2 real poles and one resonance term	32
3.6	Empirical model for long polymer using 3 real poles and one resonance term	32
3.7	Empirical model for long polymer using 4 real poles and one resonance term	33
3.8	Average cost function as number of real poles vary for longer polymer . . .	33
4.1	Trade-off between peak control input & settling time.	44
5.1	Actuator Samples and their Sizes	61

List of Figures

1.1	(a) Ionic polymer actuator before an electric field is applied; (b) Actuator after an electric field is applied	2
1.2	Chemical Structure of the Ionic Actuator Shahinpoor et al. (1998).	7
1.3	Some of the Ionic polymer actuators coated with Platinum in our lab at CIMSS.	8
2.1	Experimental setup for the measurement of open-loop tip displacement for a 1V step input.	16
2.2	Bending response of (a) 12 mm x 5 mm x 0.2 mm actuator; (b) 40 mm x 5 mm x 0.2 mm actuator for 1V step input.	17
2.3	Experimental setup for the measurement of open-loop transfer function for a 40mV random signal.	18
2.4	Magntiude and phase of the frequency response of three ionic polymer actuators.	19
2.5	(a) Change in the natural frequency of the 40mm x 5mm x 0.2mm ionic polymer actuator during the dehydration test; (b) Change in the natural frequency of the 40mm x 5mm x 0.2mm ionic polymer actuator during the rehydration test.	20
3.1	Bending response of (a) 12 mm x 5 mm x 0.2 mm actuator; (b) 40 mm x 5 mm x 0.2 mm actuator.	25
3.2	Experimental setup for the measurement of open-loop tip displacement for a 1V step input.	27
3.3	(a) Optimal curve fit using three real poles of the experimental data using for the 16 mm x 5 mm x 0.2 mm ionic polymer actuator sample to a 1 V step input; (b) Optimal curve fit using three real poles of the experimental data using for the 40 mm x 5 mm x 0.2 mm ionic polymer actuator sample to a 1 V step input.	28

3.4	(a) Cost function variation for short polymers as number of real poles vary; (b) Cost function variation for long polymers as number of real poles vary.	34
4.1	Parallel interconnection of the control model.	37
4.2	Linear Observer-Estimator compensator to track reference inputs in state space design.	39
4.3	Simulation of closed-loop tip displacement of the 7.8 mm-long polymer for varying values of the control design parameter r	43
4.4	Simulation of the control input of the 7.8 mm-long polymer for varying values of the control design parameter r	44
4.5	Root Locus representation of the closed-loop system of the short polymer.	45
4.6	Bode plot of the closed loop system of the short polymer.	46
4.7	Simulation of the tip displacement for the 26.3 mm long polymer with weighting matrix $Q = C'C$	47
4.8	Simulation of the control input for the 26.3 mm long polymer with weighting matrix $Q = C'C$	48
4.9	(a) Transfer function of the actuator at the time of the experiment; (b) Bode plot of the compensator and the system for $Q = C'C$	49
4.10	Root Locus representation of the closed-loop system of the long polymer for Case 1.	50
4.11	Bode plot of the series plant and compensator of the long polymer for Case 1.	50
4.12	(a) Simulation of the tip displacement for the 40 mm-long polymer for $Q = C'_m C_m$; (b) Simulation of the control input.	51
4.13	(a) Bode plot of the plant; (b) Bode plot of the compensator and system for $Q = C'_m C_m$	52
4.14	Root Locus representation of the closed-loop system of the long polymer for Case 2.	53
4.15	Bode plot of the series plant and compensator of the long polymer for Case 2.	54
4.16	Tip displacement of the long polymer actuator for a perturbation factor of 9% in Case 1.	55
4.17	Bode plot of the series plant and compensator of the long polymer for a perturbation factor of 9% in Case 1.	56
4.18	Tip displacement of the long polymer actuator for a perturbation factor of 9% for case 2.	57

4.19	Bode plot of the series plant and compensator of the long polymer for a perturbation factor of 9% in Case 2.	58
4.20	Variation of the Settling Time ratio as Pertubation changes($-0.3 < \Delta < 0.3$).	59
4.21	Variation of the Settling Time ratio as Pertubation changes ($-0.1 < \Delta < 0.1$).	59
5.1	Experimental setup for closed-loop control	62
5.2	Schematic of the experimental setup for closed-loop control	63
5.3	Experimental step response for the short polymer in an open-loop and closed-loop.	64
5.4	Experimental step response for the short polymer in closed-loop for various gains.	65
5.5	Experimental step response for the short polymer in unstable closed-loop at high gain.	65
5.6	Experimental step response for the long polymer in an open-loop and closed-loop.	66
5.7	Experimental step response for the long polymer in closed-loop for various gains.	67
5.8	Experimental step response for the long polymer in an open-loop and closed-loop.	68
5.9	Unstable experimental step response for the long polymer in closed-loop for high gain.	69
5.10	Experimental step response for the long polymer in closed-loop for various gains.	70

Chapter 1

Introduction

Ionic polymer actuators are a class of electroactive polymers that can be formulated to have a range of electrical properties through the chemical composition and structure of the polymers. These properties can be made to change in response to external application of electric field and/or stress. In most of the actuators, the actuator mechanism is based on the movement of an ionic species in or out of the polymer network. Different types of electroactive polymers can be characterized as gels or ionic polymer metal composites. This chapter is an introduction to the ionic polymers.

1.1 Ionic Polymer Actuators

An Ionic polymer actuator consists of a thin Nafion-117 sheet plated with gold or platinum on both sides. The actuator undergoes large deformation under moist conditions in the presence of low applied voltage across its thickness and exhibits low impedance. By applying an electric field to the membrane, ions can be moved from one surface to the other. If the actuator is placed in a cantilever configuration, and a voltage is applied across its thickness, the actuator tip bends towards the anode and then moves towards the cathode before relaxing. The ionic polymer actuator reverses its direction of bending if the voltage is reversed. The actuators have been reported to respond quickly to signal frequencies of 100 Hz by Kanno et al. (1994). The Ionic polymer actuator is also referred as the Electro-Active Polymer (EAP), Ionic Polymer-Metal Composite (IPMC), Ionic Metal-Polymer Composite (IMPC) and the Ionic Conducting Polymer Film (ICPF) in literature. These actuators are flexible, light and compact. They can be cut into any shape and size. Figure 1.1 shows

the movement of the tip of the actuator in a cantilever configuration before and after the application of 2 Volts across its thickness.

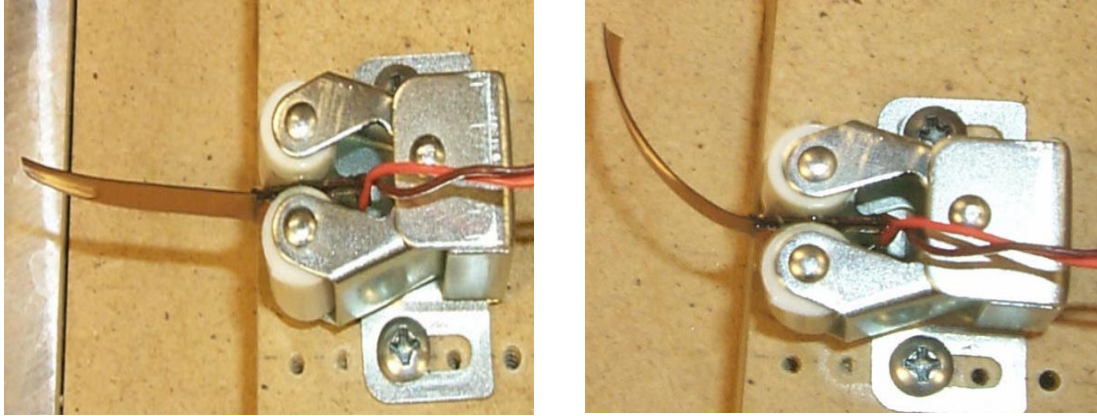


Figure 1.1: (a) Ionic polymer actuator before an electric field is applied; (b) Actuator after an electric field is applied

These ionic polymer materials can also be used as large displacement sensors. By bending the ionic polymer sensor, a voltage can be measured across its thickness. When the sensor is bent, differential stresses are induced on its layers relative to its neutral axis. This leads to a movement of ions to favored regions which can be translated into a voltage gradient which was reported in Shahinpoor et al. (1998).

1.1.1 Comparison with other Actuator Technologies

The ionic polymer actuator has a large electrically induced strain at low voltages. This property offers many advantages compared to other actuator technologies. It is very light in weight, compact, flexible, and can be cut into any size and shape. Hence it can be used in various applications such as bio-muscle, micro-robot and micro-machines.

A comparison of the ionic polymer actuator with other conventional technologies such as PZT, PVDF and Shape Memory Alloys is shown in Table 1.1 which was reported by Hunter and Lafontaine (1992). By examining the stress and strain values, we observe that the actuators providing the largest displacements exhibit low stress. Shape Memory Alloys(SMA) and hydraulic actuators demonstrate large stress and strain capability. However, SMAs are mechanically inefficient, due to poor conversion of thermal energy into mechani-

cal energy. Hydraulic systems offer good efficiency, but the large overhead equipment such as pumps and piping impacts their applicability for small scale devices. The ionic polymer generates a high strain as compared to any other actuator technologies and can be used as a high displacement actuator and sensor. The table also illustrates the similarities between the ionic polymer actuator and the human muscle. Active research is going on in the field of ionic polymers to use these actuators as artificial muscles [Wax and Sands (1999)].

Table 1.1: Comparison of Actuator Technologies

Actuator Technology	Maximum Strain (%)	Maximum Stress (MPa)	Maximum Efficiency (%)	Bandwidth (Hz)	Relative Speed (full cycle)
Pneumatic	0.5	0.7	> 90	20	fast
Hydraulic	0.5	70	> 80	4	fast
PZT	0.2	110	> 90	5000	fast
PVDF	0.1	4.8	n/a	5000	fast
SMA	> 5	> 200	< 10	3	slow
Muscle	> 40	0.35	> 35	10	medium
Ionic Polymer	> 40	0.3	> 30	10	slow

One of the disadvantages of using the ionic polymer is that the force output of the actuator is much less than a PZT or a PVDF actuator. Another disadvantage of using the ionic polymer as an actuator is its low bandwidth which is two orders less than PZT or a PVDF technology. By increasing the force output and the bandwidth of the ionic polymer, it can be used for microactuation and bio-mimetic applications. Many researchers are studying methods to improve the force output by varying the method of preparation of the ionic polymer actuator.

1.2 Motivation

One of the disadvantages of ionic polymer materials is that their settling time to a step voltage is on the order of 5-20 seconds. The slow time constant of an ionic polymer actuator limits the actuation bandwidth. Previous results have illustrated that cantilevered actuators of size 15mm x 2mm x 0.184mm (unsupported length of 10mm) have settling times in the order of 4-10 seconds [Kanno et al. (1996b), Kanno et al. (1996a) and Tadokoro et al. (2000)]. Due to this limitation, many applications will not be able to make use of the large

displacement effectively because of the limited bandwidth of the actuator. This research work aims to increase the bandwidth of the ionic actuator by designing a controller using state space methods. The controller is designed to reduce the settling time and the overshoot of the actuator. By using a suitable control algorithm, the ionic polymer actuator can be used to actuate signals of high frequency.

1.3 Literature Review and Background

1.3.1 Modeling

The physical phenomenon responsible for exhibiting high strains in the actuator is not completely understood. Several plausible models have been suggested by various research groups in this field. Physical phenomenon, such as ionic motion, water back diffusion, electrostatic force, concentration gradient etc. have been considered as forces responsible for the bending. Yet, no clear set of principles have been able to explain the motion of the polymers completely.

One of the first models proposed in this field was the theory of nonhomogeneous large deformation of Ionic polymeric gels in electric and pH fields by Shahinpoor (1993). Two distinct mechanisms were identified to be responsible for the bending of the ionic polymeric strips. The first mechanism, the presence of pH field, distributes the anions and cations within the gel network creating a spatial distribution of the ions. The second mechanism, the application of electric field across the thickness, causes the bending of the ionic polymer towards the anode or the cathode depending on the initial spatial distribution of the ions. The microelectro-mechanics of ionic polymeric gels used as synthetic robotic muscles was reported by Shahinpoor (1994b). The model presented by Shahinpoor in the paper considers the effect of the internal electric charge redistribution of fixed and mobile ions due to the presence of the electric field.

At the same time, an empirical model and the characteristics of the ionic polymer actuator was presented by Kanno et al. (1994). The step response of the actuator was empirically modeled as a linear combination of real poles. The parameters in the transfer function, which are the set of real poles and their coefficients, were optimized using a least square method and reported for a varying range of voltage input. The step response under constant voltage was expressed by a transfer function of the fourth degree by this

dynamic model. Kanno et al. (1996b) proposed the ‘black-box model’. The ionic polymer was modeled as a series capacitor and resistor network. Three stages: the electric stage, the stress generation stage and a mechanical stage were identified to be responsible for the bending of the actuator. An extension of the two dimensional model was proposed by Kanno et al. (1996a), considering the three dimensional network and the effects of the curling at the end of the actuator. In both the above papers, the mechanical stage was modeled using a finite element model.

A study of an ionic metal composite sensor was presented in Mojarrad and Shahinpoor (1997). The characteristics of the sensor films was studied as a function of the displacement applied to the tip. It was observed that the voltage output was highly linear in one direction of the tip displacement input and a higher order polynomial was required to describe the voltage output for the negative displacement. Similarly, the vibration and resonance characteristics of several ionic polymeric membrane metal composites was presented by Mojarrad et al. (1997). It was observed here that as the applied frequency was increased, the maximum deformation observed also increased till a critical frequency, after which it decreases. The factors affecting the membrane composite performance were also identified as the amplitude and frequency of the applied voltage and dehydration.

Shahinpoor (1999) presented the electromechanics of the ionic-beams to be used as artificial muscles. A mathematical model, similar to the Euler-Bernoulli model, was developed to include the non-homogeneous distributed electrically-induced moment due to the presence of a non-homogeneous electric field in an elastic material. The effects of the two driving forces, electrostatic force and water pressure gradient and two fluxes, electric current and water current, on the behavior of the ionic gels was presented by de Gennes et al. (1999).

A mathematical model which tries to explain the behaviour of the IPMC is presented in Shahinpoor et al. (1998). This paper reviews the various research activities of the ionic polymer. The sensing and actuation capabilities, vibrational and resonance characteristics of the ionic polymer are reported. A brief description of the preparation and applications of ionic polymers is also presented. Four forces produced by ionic motion are used to model the ionic polymer-metal composite in Shahinpoor (1998). The model presented in this paper, considers the redistribution of fixed ions and migration of mobile ions within the network on the application of an electric field. Factors such as hyperelasticity, concentration of ions

and electromechanical coefficient were used to describe the bending motion. The cryogenic properties and load characteristics are reported in this paper.

Tadokoro et al. (2000) presented the ‘white-box model’ of the Nafion-Pt composite actuators. The model consisted of two stages: An ionic migration model, in which the movement of sodium ions and water ions is modeled and a stress generation model, in which the swell and contraction of membrane, momentum effect, electrostatic force and conformation change of the membrane is included. The quadratic relation between the step voltage and maximum displacement was shown in this paper.

Nemat-Nasser and Li (2000) presented a model considering the microstructure of water-saturated Nafion. A phase separation morphology considering the hydrophilic and hydrophobic regions which composed of ionic groups and counter ions was used to explain this model. The model proposes that due to electrostatic interaction, application of an electric field, redistribution of the ionic groups, and redistribution of water molecules, the differential swelling of the membrane causes the bending movement.

An empirical model was presented by Mallavarapu et al. (2001) in which a simple pole zero model was used to model a short ionic polymer actuator. A feedback controller was designed to reduce the settling time and decrease the overshoot of the short polymer in a cantilever configuration. The implementation of the controller at large gains was hindered by the resonance frequency of the polymers.

1.3.2 Summary

None of the above models presented in literature completely explain the motion of the polymers. Most of the models presented use partial differential equations to explain individual physical phenomenon. These differential equations were not coupled with other physical phenomenon and solved for a set of solutions. In some other papers, a finite element method was used to obtain the displacements. Such a physical model cannot be used for the design of the controller because it is incomplete.

The empirical model can be used as a control model due to its simplicity of implementation. The empirical model presented in literature does not incorporate any resonance effects seen in the longer polymers. Hence it had to be modified before using as a control model. No literature was present in the field of control of ionic polymers to improve their performance or increase its bandwidth by designing a controller.

1.3.3 Preparation

The ionic polymer is a perfluorinated ion exchange membrane such as Nafion-117 (DuPont, U.S.A) and is given an electroless plating with a metal such as gold or platinum. The chemical structure of the of the ionic polymer is shown in Figure 1.2 where n is such that $5 < n < 11$ and $m \sim 1$ and M^+ is the counter ion (H^+ , Li^+ or Na^+) as reported by Shahinpoor et al. (1998). This ionic polymer actuator has an ability to absorb large amounts of polar solvents such as water. Platinum ions are dispersed through out the hydrophilic regions of the polymer are reduced to corresponding metal atoms resulting in the formation of dendritic type electrodes.

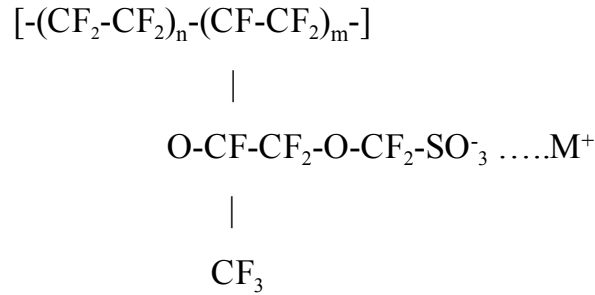


Figure 1.2: Chemical Structure of the Ionic Actuator Shahinpoor et al. (1998).

The ionic polymer can be prepared in different ways. Chemical plating or electroless plating is a the most common method of preparation of these polymers. In the chemical plating method suggested by Oguro et al. (1999), an ion-exchange of the counter ion such as Na^+ with a cationic solution (gold complex) is followed by a reduction process in an aqueous solution of reducing agents such as sodium sulphate. This ion exchange and reduction process can be repeated several times until a suitable thickness of the electrode is plated on to the surface of the membrane. The sodium cation in the composite is then exchanged with various alkali metal ions by immersing the composite in chloride salt solutions overnight. Thin films of the electrodes have been formed by a electrostatic self assembly process by combining metal nanocluster particles with or without polymer interlayer spaces, presented in Yanjing et al. (1999).

Figure 1.3 shows 2 actuators prepared in our lab at CIMSS, where Nafion-117 mem-

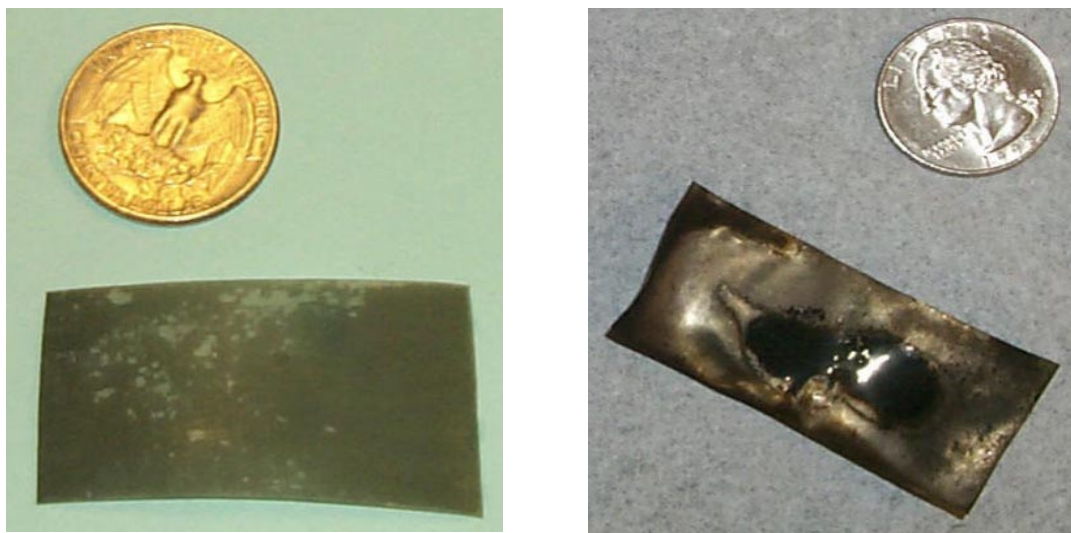


Figure 1.3: Some of the Ionic polymer actuators coated with Platinum in our lab at CIMSS.

brane was coated with Platinum using the chemical plating method. Recently at CIMSS, efforts of researchers have focussed on new ways to manufacture these membrane actuators, which constitutes applying the metal electrodes to each side of the Nafion membrane, as explained by Bennett (2001).

The two methods that have been studied are sputter coating and electroless plating. Sputter coating uses gas plasma to directly deposit thin metallic films and is commonly used in electron microscopy. A variety of metals can be deposited using this method, including gold, platinum, titanium, nickel, and silver. However, the process takes place under a vacuum at slightly elevated temperature. This means that the membrane must be dry prior to the coating process and then hydrated after. Besides the handling issues that this raises, some other problems have been encountered as a result of this. The electrodes deposited by sputter coating have been observed to become much more resistive after hydration. This has been attributed to the fact that the membrane swells when hydrated, thus pulling the grains of the metal electrode apart and increasing the resistance of the bulk metal.

Another method that has been explored is electroless plating. Electroless plating is a process by which metal ions in solution are reduced to elemental form by a reducing agent directly on the surface of a part. In the case of some metal parts this can be done without a catalyst. In the case of plastic parts the surface must be catalyzed for the reaction to occur. The electroless plating process that has been developed consists of an

initial deposition of a very thin layer of palladium to serve as a catalyst for the reduction reaction. The part is then placed in a bath of nickel chloride and sodium hypophosphite at elevated temperature until the desired thickness of metallic nickel is formed on the surface. Some issues that have been encountered with this process are adhesion and degradation of the electrode. Early samples had electrodes that would flake off very easily, though this problem seems to have been solved by increasing the surface roughness of the membrane prior to plating. The resistance of the electrodes has also been observed to increase over time with the samples stored in de-ionized water, but “as-plated” resistances as low as 2-3 Ω/cm have been observed. Although it is not as easy to change metals as with the sputter coating process, other metals besides nickel can be electroless plated. Examples are copper and silver. The electroless plating process has the advantage that all of the process steps occur in aqueous baths, so the part may remain hydrated throughout the entire procedure.

The next step in the investigation of the manufacture of these actuators is to incorporate electroplating into the process with the goal of producing electrodes with lower surface resistance and to perform a study using surface roughness as a parameter to determine how the apparent charge density affects the performance of the actuators.

Takenaka et al. (1982) studied the electrocatalysts and their plating methods to perfluorosulphonic acid polymers membranes. In this method, Nafion membrane was clamped between two chambers of a reactor. Platinum solution (Pt salt, platinic acid) was present in one chamber and a reducing agent was present on the other side. The reducing agent penetrates through membrane to reduce Pt solution to Pt metal. Noble metals and alloys were attached to both sides of the membrane without a binder using chemical reactions of metal salt solutions in the presence of a reducing agent. This method is the most common type of electroless plating used in the preparation of ionic polymer actuator.

Lawrance and Wood (1980) proposed the hot pressing method. Here the catalyst is deposited upon the surface of the polymer electrolyte upon the roughened surface and fixed by means of pressure or heat. The amount of catalyst normally required for making the process is reduced by this method. Three chemical techniques of preparation of ionic polymer metal composites was reported by Liu et al. (1992). The Takenaka-Torikai method, Impregnation method with and without equilibrium was compared and characterized visually by transmission electron microscopy to study the polarization and hydrogen adsorption of the various methods.

1.3.4 Applications

Ionic polymer research has experienced rapid development in the last decade. Mostly applied to design and develop medical and micro-machines, its similarity to human muscle has stirred a lot of interest.

One of the first applications of the ionic polymer actuator is presented in Shahinpoor (1994a). In this paper, a spring loaded actuator was designed and a mathematical model was presented for the dynamic response of the contractile fibers embedded in the elastic springs. By applying an electric field, the polymer gel fiber bundle is made to contract or expand. A mathematical model, based on the proposed composite structure taking into consideration various physical phenomenon such as pH of the gel and surrounding medium, hyperelasticity of the fiber bundle and dimensions, and simulation and experimental data were presented in this paper.

A micro catheter with active guide wire that has two bending degrees of freedom was designed using the ICPF by Guo et al. (1996). The active guide wire consisted of micro hollow cable and the actuator was fixed by bonding. The performance of system was evaluated by application of electricity in physiological saline solutions.

The ionic polymer actuator was used as a servo actuator in the development of a capsule micropump by Guo et al. (1997). The micropump made use of two active one-way valves which make use of the same actuator and supply tank. The proposed actuating mechanism was simple and the micropump had satisfactory responses. This type of micropump can supply micro liquid flow and could be used for diagnosis and surgery in medicine. A number of experimental results were also reported in Guo et al. (1999).

An elliptical friction drive actuator was also developed by Tadokoro et al. (1997) which generates an elliptic motion for use in ultrasonic motors. A pattern plating method was developed in order to produce multiple ICPF actuators and a bridge combining the actuator motions at the same time. The friction drive was used as a driving device. When sinusoidal voltages with a phase difference are applied to the actuators, the top of the arch makes an elliptic motion. The relation of the elliptic motion to the applied voltage was reported in this paper. A similar device with multiple degrees of freedom was presented by Tadokoro et al. (1999). A micro motion device was developed by crossing a pair of planar devices perpendicularly at the end points using parallel mechanism of the actuators. The

actuator motion and the forces and moments applied were explained using the compliance matrix.

Biomimetic fish-like propulsion using the ICPF was also replicated by Mojarrad and Shahinpoor (1996) and Guo et al. (1998). The ICPF actuator was used as fins of the fish and the speed of the fish was varied by changing the frequency of the sine wave excitation. Such a type of fish propulsion system can be used for in-pipe inspection and microsurgery of blood vessels. The structure of the microrobot and the motion mechanism is explained.

Linear and platform type robotic actuators were made by attaching the ionic polymer actuators from end-to-end and in a movable platform in a cylindrical configuration by Karim Salehpoor and Mojarrad (1997). A theoretical model was developed and the simulations were compared to the experimental results. The electrodes were embedded within the platform to convert the bending response of the actuator into a linear motion of the mobile platform.

Cohen et al. (1998) developed a low mass robotic arm using electroactive polymers which can be used in future NASA missions. Space mechanisms require light weight and compact actuators and sensors which are driven by low power. Mechanism such as a gripper, manipulator arm and a surface wiper were successfully developed and tested. These mechanisms exhibited superior actuation displacement, low mass, low cost and low power consumption.

By designing a controller, many applications can have a control network which will enhance the performance of these actuators by reducing the settling time and increasing the bandwidth to actuate high frequency signals.

1.4 Overview of Thesis

1.4.1 Research Objectives

The objectives for this research can be summarized as:

1. To experimentally obtain a series of step responses and transfer functions for various lengths of the ionic polymer actuator,
2. To empirically model the ionic polymer actuator by optimization methods and obtain a state space representation suitable for control design,

3. To design a controller using LQR techniques to reduce the settling time and decrease the overshoot of the closed-loop system compared to an open-loop response ,
4. To implement the controller on the ionic polymer actuator and compare the results to the simulation.

1.4.2 Contribution

The following is a list of contributions made in this work:

- The step response of the ionic polymer actuator is studied in a cantilever configuration. The importance of control of resonance is stressed by studying the frequency response data of three different sizes of the polymer. The change in the natural frequency as the ionic polymer dehydrated and re-hydrated is quantified.
- An empirical model is developed and generalized for any length of the polymer. Resonance terms are included to model the resonance seen in longer polymers. The accuracy of the empirical model as a function of the number of real poles in the model is studied for a short and long polymers.
- A linear observer-estimator controller is designed using the LQR techniques which reduced the settling time and the overshoot in closed-loop simulations. The response and stability of the closed-loop system for a long ionic polymer actuator is studied for two different cost functions.
- Experiments are conducted on the closed-loop ionic polymer actuator system. Faster settling time and reduction in overshoot in the tip displacement are observed by using feedback control. The closed-loop system of the ionic polymer actuator went unstable at high values of the design parameter r , as predicted by the simulations, due to the change in resonance frequency as the polymer dehydrates during testing.

1.4.3 Approach

Chapter 2 presents the inconsistency exhibited and the change in first elastic resonance as the polymer gets hydrated and dehydrated. The challenges posed by this inconsistency and the need for a robust controller to overcome it, are documented in this chapter.

Chapter 3 discusses the development of the empirical model. The empirical model is based upon the experimental data of a series of open-loop responses of the ionic polymer actuator to a unit step voltage. An empirical model presented by Kanno, R.(1994) is modified and optimized using the least square method and a transfer function is developed. The method of optimization and the analysis of the cost function as the number of real poles vary is presented.

Chapter 4 introduces the feedback control algorithm used to design the controller. The transfer function obtained after optimization is converted into a canonical state space representation. The state space model does not have any physical significance, but the states are ordered such that it is easy to distinguish the various time constants of the response with the resonant dynamics. A study on the number of real poles required to accurately model the system is made by performing the optimization for an increasing number of real poles is also documented. The behavior of the ionic polymer actuator is also explained on the basis of the location of the poles and shown by a root locus plot. The design of the linear observer estimator controller using LQR method is explained.

Chapter 5 discusses the experimental setup and the results of the closed-loop control of both a short polymer and a long polymer. The reduction in the settling time and the control input is presented in this chapter. The difference between the simulations illustrated in *Chapter 4* and experimental results is explained.

Finally, *Chapter 6* summarizes conclusions, proposes future work and formulates the corresponding recommendations.

Chapter 2

Dynamic Response of Ionic Polymer Actuators

The ionic polymer actuator shows a very large deformation in the presence of low applied voltage. In this chapter, the dynamic response of the actuators when a step voltage is provided is discussed. First, the previous work conducted by Shahinpoor and Kanno is presented. The dynamic response analysis conducted as a part of this research is discussed. The step response of the polymer is shown which indicates a slow settling time and a fast rise time. The long polymers exhibit resonance during the first few seconds of the response. A study of the change in the natural frequency is also presented. The variation in the natural frequency as the unsupported length of the polymer increases is discussed. It is also seen that the natural frequency of the polymer varies as the polymer hydrates and dehydrates.

2.1 Previous Work

The dynamic response of ionic polymer actuators has been studied previously by Kanno (1994,1996) and Shahinpoor (1997). In their work, a series of tests on the IPMC sample of size 20 mm x 4 mm in a cantilever configuration were conducted. In the first test, an alternating signal was applied to the actuator, and the measurement of the tip displacement was taken as a function of frequency. It was observed that the IPMC sample could follow the input signal very closely up to a frequency of 35 Hz. Resonance of this sample was observed at a frequency of 20 Hz and the associated displacement was 7.5 mm. The actuator was

also tested after encapsulating it in a plastic membrane, Saran. The displacement observed was less than the previous case due to increased stiffness of the encapsulating membrane.

In the second test, the displacement of the free end was measured by varying the amplitude of the sinusoidal input voltage from 0.5 Volts to 2.5 Volts at a constant frequency of 0.5 Hz. It was observed the relation of the displacement to the amplitude of the free end was linear in the given range of voltages at constant frequency of 0.5 Hz. In the next test, the variation of deformation was measured with the imposed voltage gradient for varying frequency. The lowest frequency of 0.1 Hz caused higher deformation at high voltages than the frequency of 1 Hz at high voltages. As the frequency increased, the deformation at higher voltages tends to be constant.

Most of the previous work in dynamic response analysis concentrates on a single size polymer. For various applications, the length of the polymer can vary. Hence the nature of the dynamic response as length varies is studied as a part of this research work. The step response of a short polymer is reported in previous work. The step response of a longer polymer and whether the response varies as a function of the hydration level has never been studied. This chapter aims to study the dynamic response of a set of polymers with varying length, and the effects of hydration and dehydration on their behavior.

2.2 Step Voltage response

2.2.1 Test Setup

To study the dynamic response of the ionic polymer material samples given, a test setup was built. The test setup consists of a set of two electrodes placed at the fixed end of the actuator. The sample is cantilevered from the electrodes and the displacement at approximately the tip of the actuator is measured with a laser vibrometer. The actuator is excited by a voltage supplied by a power amplifier (50 V, 1.2 A) that is controlled by the signal from a digital signal processor (dSPACE, Inc. Model 1102). The digital signal processor also measures the actuator displacement at the tip, the voltage across the actuator, and the current through the actuator. Figure 2.1 is a schematic of the test setup. The three different sizes of the ionic polymer actuator used in this set of experiments are summarized in Table 2.1.

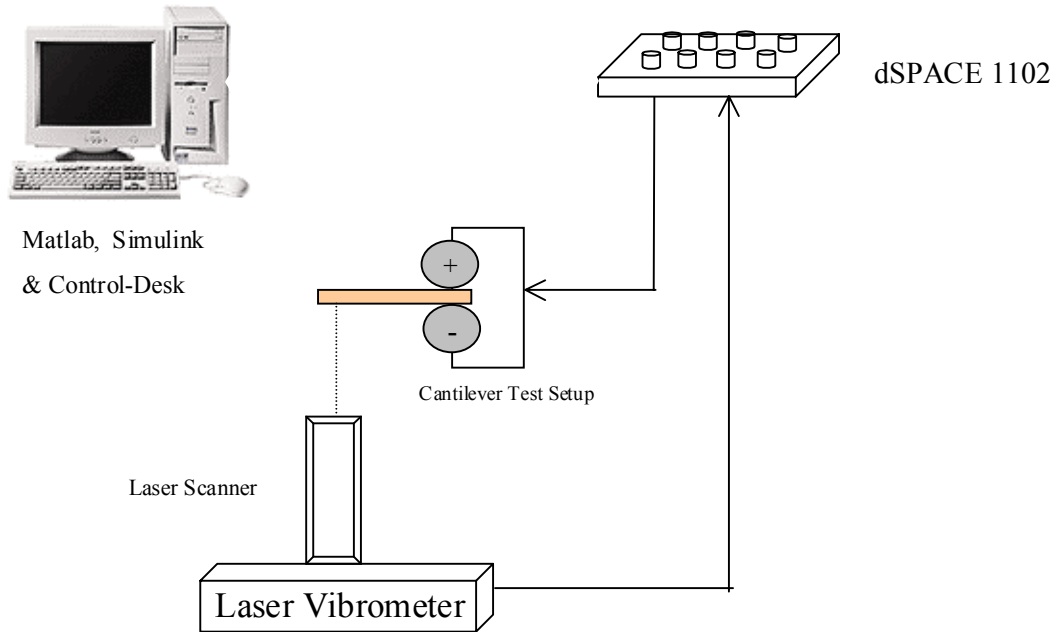


Figure 2.1: Experimental setup for the measurement of open-loop tip displacement for a 1V step input.

Table 2.1: Actuator Samples and their Sizes

Actuator Label	Length (mm)	Width (mm)	Thickness (mm)	Unsupported Length (mm)
Short	12	5	0.2	7.8
Medium	30	5	0.2	16.7
Long	40	5	0.2	26.3

2.2.2 Experimental Results

Application of a step voltage across the thickness of the membrane causes a bending in the short polymer, as shown in Figure 2.2a. The step response of the polymer is characterized by a fast rise time, on the order of 0.05 seconds, and a slow relaxation to a steady-state position. The time constant of the relaxation is at least an order of magnitude larger than the rise time. Our experiments on several polymer actuators indicate a relaxation time on the order of 5-15 seconds.

Another defining characteristic of the actuator response is the large ratio of the peak response to the steady-state response. Figure 2.2a illustrates that the peak response of the polymer is over $200 \mu\text{m}$ whereas the steady-state response is on the order of $50 \mu\text{m}$. Previous

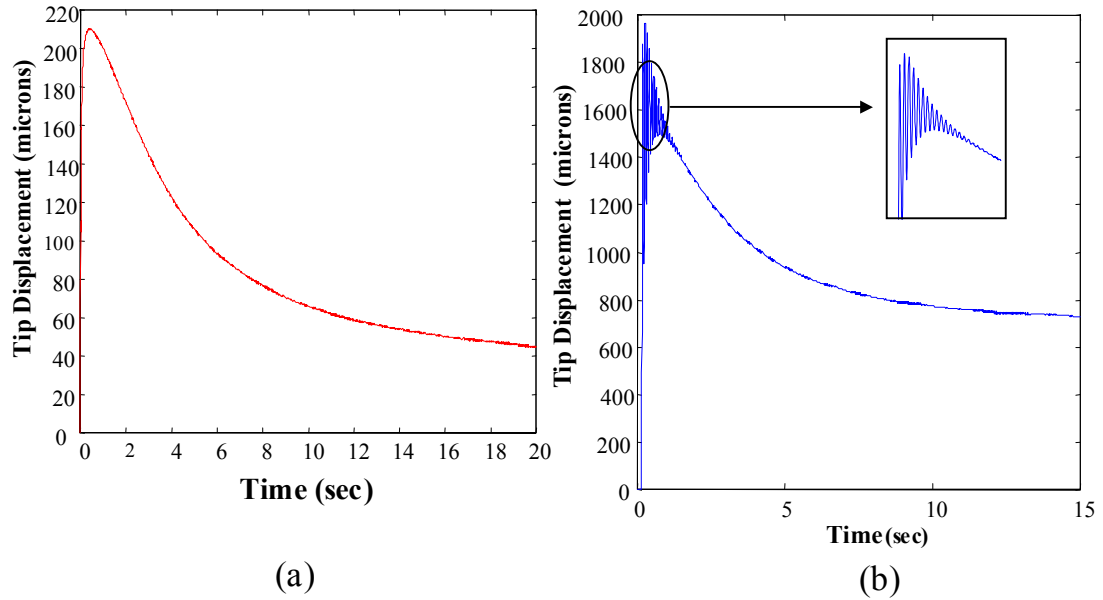


Figure 2.2: Bending response of (a) 12 mm x 5 mm x 0.2 mm actuator; (b) 40 mm x 5 mm x 0.2 mm actuator for 1V step input.

researchers have correlated the initial rise to the application of the electric field and the slow relaxation to the back diffusion of water within the polymer (Tadokoro, S., 2000).

Increasing the length of the actuator introduces another response mechanism due to the decrease in the resonance frequency of the actuator. Figure 2.2b is a plot of the tip displacement of a cantilevered sample of length 40 mm x 5 mm x 0.2 mm with an unsupported length of 26.3 mm. The steady-state response is greater than the steady-state response of the shorter sample by over a factor of 10, and the response exhibits a 2.5:1 ratio of peak response to steady-state response. The inset of the figure demonstrates the oscillations that occur in the first 2-3 seconds of motion. These oscillations are caused by the resonance of the actuator.

2.3 Transfer functions

2.3.1 Test Setup

The dynamic response of the ionic polymer was studied using transfer functions. The ionic polymer actuator sample is placed in a cantilever configuration in a small test fixture as shown in Figure 2.3. The deflection of a point near the tip is measured with a laser vibrom-

eter and a Tektronix 2630 Fourier Analyzer is used to compute the frequency response. A DC coupled 40mV random signal is used as the excitation signal. The test setup is shown in Figure 2.3. Three different sizes of the ionic polymer actuator were used in this set of experiments, summarised in Table 2.1.

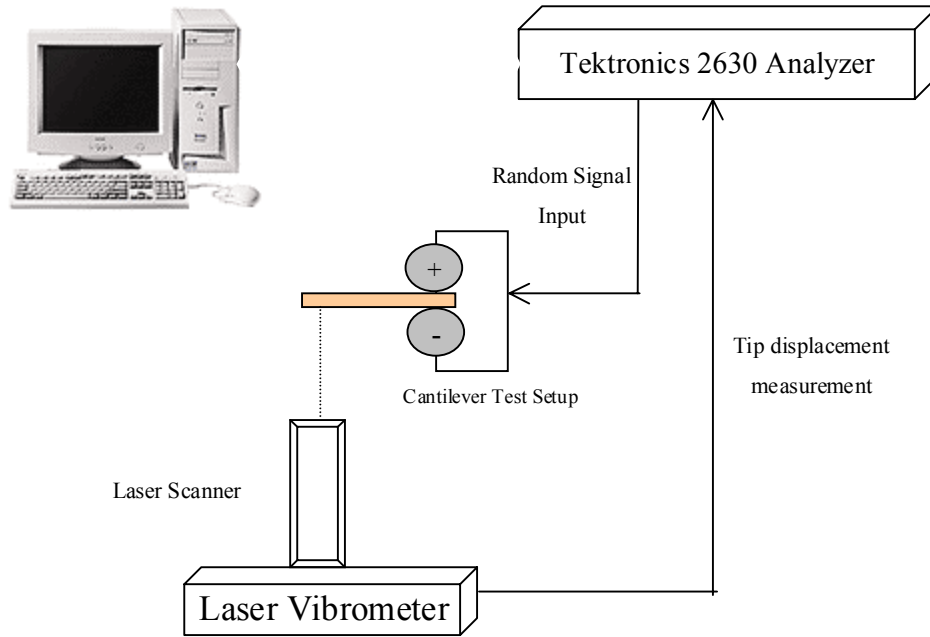


Figure 2.3: Experimental setup for the measurement of open-loop transfer function for a 40mV random signal.

2.3.2 Experimental Results

Figure 2.4 shows the frequency response data for the 3 different lengths of ionic polymer actuators listed in Table 2.1. All three samples were provided to us by Dr. M. Shahinpoor and Dr. K. Kim of The University of New Mexico. The measurements demonstrate that the frequency response below 5 Hz is relatively constant in magnitude and exhibits a phase lag that increases towards 90 degrees for increasing frequency. The sharp increase in magnitude and abrupt 180 degree phase lag is due to resonance of the polymer. From Figure 2.4, we can infer that the natural frequency of actuator decreases as the length of the polymer increases similar to dynamics of a cantilever beam. Hence, control of resonance should be given more importance as the length of the polymer increases. Since all the experiments were conducted in air, the damping of the ionic polymer actuator is much lower than that

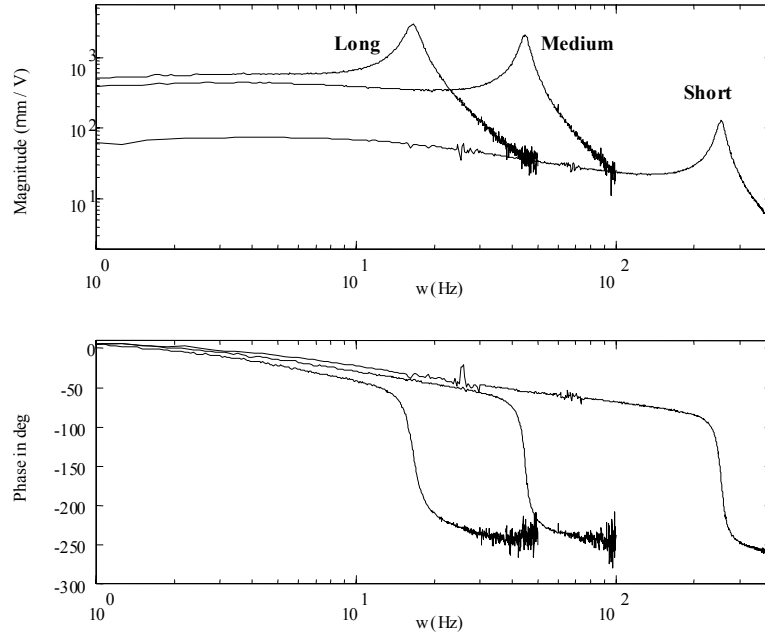


Figure 2.4: Magntiude and phase of the frequency response of three ionic polymer actuators.

observed in water.

A cantilevered structure will have a resonance frequency that is a function of the structural geometry and material properties. An attribute of ionic polymer actuators that has been reported previously is that the stiffness of the actuator is a function of the hydration of the polymer [Shahinpoor et al. (1997)]. Variations in stiffness introduce variations in the resonant response of the actuator. Difficulties in controlling the hydration and the fact that the hydration might change with respect to time results in inconsistencies in the mechanical response exhibited by the polymers during continual use.

To assess the importance of these factors on the resonance frequency of a long ionic polymer actuator, a series of tests are performed to determine the effect of material hydration on the resonance frequency of the polymer. The tests are performed on the longer ionic polymer sample of size 40mm x 5 mm x 0.2 mm (unsupported length of 26.3 mm). Two tests involving the effect of de-hydration and re-hydration are performed in air.

In the first test, the ionic polymer actuator is continuously excited and a frequency response is taken every 2 minutes to study the effect of de-hydration and continual use on the first resonance frequency of the polymer. In the second test, the ionic polymer actuator is hydrated by boiling it in de-ionized water for 30 minutes and the frequency response data

is taken. After some time, the actuator is removed from the fixture, hydrated in the same manner and a frequency response test is performed again. This tested the consistency of the frequency response as a function of handling (i.e. removing from the test fixture) and boiling.

Figure 2.5a shows the transfer functions taken for the first series of tests. A change in the natural frequency is seen as time progresses. On close observation, it is seen that the natural frequency changed from 17 Hz to 19.13 Hz in a span of 8 minutes. This represents a 12.5% change in the natural frequency due to changes in the hydration state of the polymer. The change is attributed to the change in hydration because a noticeable change in color is observed on the surface of the polymer.

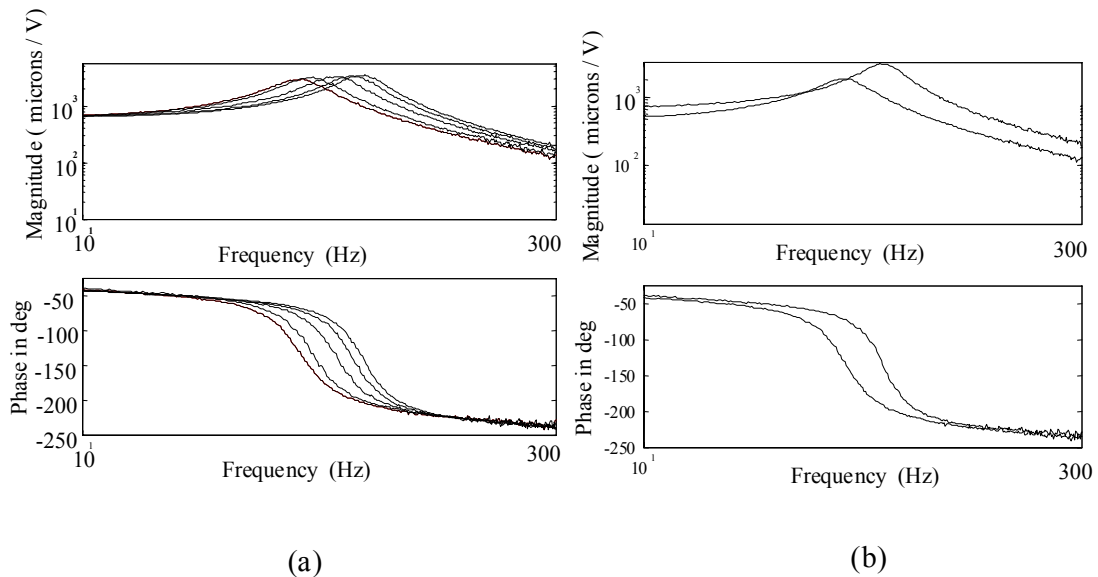


Figure 2.5: (a) Change in the natural frequency of the 40mm x 5mm x 0.2mm ionic polymer actuator during the dehydration test; (b) Change in the natural frequency of the 40mm x 5mm x 0.2mm ionic polymer actuator during the rehydration test.

In the second frequency response test, it is hypothesized that the natural frequency of the ionic polymer actuator might remain the same if the material is rehydrated after a period of continual use. Contrary to the hypothesis, Figure 2.5b shows a change in the natural frequency between tests. It is seen that the natural frequency changed from 17 Hz to 18.13 Hz, a change of 6.6% in the first elastic resonance. It is also noted that the quasi-static response of the polymer changed significantly between tests. This is illustrated by

the change in the magnitude of the frequency response at frequencies well below resonance.

This change in the natural frequency in the first case is attributed to the increasing stiffness of the polymer due to dehydration and/or inconsistencies in the preparation of the polymer. In the second test, it is attributed to the inconsistencies in the preparation of the polymer or the effect of inconsistent boundary conditions at the fixed end. In either case, we see that 5-15% changes in the natural frequency of the polymer are possible from continual use or from variations between tests performed in this work. The magnitude of the change in natural frequency does not represent the entire population of the samples tested, since a statistical analysis is not presented. The change in the natural frequency is given more importance. This result necessitates the design of feedback control laws that are robust with respect to these percentage changes in the natural frequency of the actuator.

2.4 Summary

In this chapter, the dynamic response of the ionic polymer actuator was discussed. On application of step voltage across the thickness of the actuator, a fast rise time and a slow relaxation to the steady state was observed. High overshoot can also be observed due to the ratio between the peak response and steady state value. For a longer polymer actuators, oscillations due to resonance was observed during the first few seconds of the step input. The frequency response data for 3 different lengths of the actuator illustrates that the natural frequency of actuator decreases as the length of the polymer increases.

The variation in stiffness due to changes in hydration was studied. The de-hydration test shows a change of 12.5% in the natural frequency due to the effect of de-hydration and continual usage on the first resonance frequency is reported. In the second test, the natural frequency of the polymer changed by 6.6%, though it was hypothesized that the natural frequency of the actuator might remain the same if the material is rehydrated after a period of continual use.

Difficulties in controlling the hydration and the change of hydration as time progresses might result in mechanical inconsistency. Hence, the importance of the need for control, to shape the dynamic response of the actuator is stressed in this chapter.

Chapter 3

Empirical Modeling

The ionic polymer actuator behavior is explained by physical phenomenon in many plausible ways. None of these models are suitable for control. In this chapter, the empirical model of the ionic polymer is developed. First, an empirical model developed by Kanno is modified and generalized for any length of the polymer. Then, the model is optimized using a function in MATLAB. The accuracy of the curve-fit obtained is a function of the number of real poles included in the empirical model. Hence an analysis of the cost-function variation as the number of poles is varied is discussed.

3.1 Introduction

Many physical models were presented to explain the high displacement of the ionic actuator in cantilever configuration at low voltages. In the last four years, research in this field has intensified, with many macro level and micro level models being considered. Physical phenomenon such as ionic motion in the polymer, water back diffusion, applied electrostatic force, concentration gradient of the ions, etc. have been considered as some of the forces responsible for the bending of the actuator. Yet, no clear set of principles have been able to explain the motion of the polymers completely.

An empirical control model does not consider any physical phenomenon. It is a simple linear combination of real poles and imaginary poles useful for designing feedback controllers. The empirical model is obtained by studying the tip displacement of the ionic polymer actuator to a given step input. The poles and their coefficients in a transfer function, are optimized by defining a cost function such that the error between the experimental

data and the simulated step response of the actuator is reduced. An input-output transfer function of the ionic polymer actuator is obtained and a state space model is developed from the transfer function. The output of the transfer function is the tip displacement and the input to the transfer function is the control voltage. The states in the model do not have any physical significance, but we will order the states in such a manner that it is easy to distinguish the various time constants of the response with the resonant dynamics.

Modeling of ionic polymer actuators for the purpose of control is complicated by the fact that the dominant period of the dynamic response is greater than 1 second. Most commercially-available frequency analyzers are limited to analyzing frequencies greater than 0.5 or 1 Hz. Furthermore, testing at frequencies less than 1 Hz requires long sample records to obtain high frequency resolution (e.g. a record with 1024 points sampled at 2.56 Hz would require 400 seconds of data). Averaging the data would increase the test time even further, making problems due to dehydration in the material even more pronounced.

In this research, the empirical model developed by Kanno et al. (1994), is modified and used for controller design. Later in 1996, Kanno, R., proposed the black box model, in which a second order delay was incorporated into the stress generation stage. A similar term is used to modify the resonances observed in the longer polymers in this research. A key element in this research is whether or not feedback control laws can be designed using a linear time invariant dynamic model of the polymer.

3.2 Empirical model by Kanno et al. (1994)

In the paper presented by Kanno et al. (1994), the authors consider the motion dynamics as a linear phenomenon. Step response of the ionic polymer actuator in a cantilever configuration for a constant voltage was approximated by a fourth degree polynomial. The step response $y(t)$ of a 15 mm x 2 mm x 0.182 mm ionic polymer actuator in a cantilever configuration with unsupported length of 10 mm was approximated as,

$$y(t) = ae^{-\alpha t} + be^{-\beta t} + ce^{-\gamma t} + de^{-\delta t} + e \quad (3.1)$$

where α , β , γ , and δ represent time constants of the response, and a, b, \dots, e represent the coefficients. Each of the parameters was identified using the least square method and

a transfer function was developed. A table of the identified coefficients and time constants for a range of step voltages from 0.5 Volts to 1.5 Volts was presented in this paper.

Generalizing equation (3.1), we assume that the response to the control input $u(t)$ is expressed in the Laplace domain as

$$G(s) = \frac{Y(s)}{U(s)} = \frac{a}{s + \alpha} + \frac{b}{s + \beta} + \dots \quad (3.2)$$

In the work by Kanno, et al, the unsupported length of the ionic polymer actuator was smaller and the response did not exhibit any contribution due to resonance. The fourth degree transfer function was validated by observing the simulation and experimentation of the response of the ionic polymer actuator to series of square waves (1.5 V and 0.1, 0.5, 1.5 Hz).

The empirical model presented in this work is one of the first and most useful for a control model. However, as discussed in *Chapter 2*, resonance should be given more importance as the length of the polymer increases. In this research work, the above model is modified to incorporate resonance and use it as a control model.

3.3 Modification of the Empirical Model

In our work, the empirical model is based on the experimental data of a series of open-loop responses of the ionic polymer actuator to a unit step voltage. Figure 3.1a shows an open loop response for a 26.3 mm x 5mm x 0.2mm. Figure 3.1b shows an open loop response for a 7.8 mm x 5 mm x 0.2 mm ionic polymer actuator. The response of the long and short polymers exhibit a fast rise time but a slow decay to steady state value. In the longer polymers, resonance appears to be dominant in the first few seconds of the response, dying out as the steady state value is reached, as shown in the inset in Figure 3.1a.

In this paper, equation (3.2) is modified to incorporate the resonance modes as shown in the frequency response of the ionic polymer actuator. The model with resonant terms can be represented in the Laplace domain as

$$G(s) = \frac{Y(s)}{U(s)} = \frac{a}{s + \alpha} + \frac{b}{s + \beta} + \frac{c}{s + \gamma} + \dots + \frac{K_{r1}\omega_{n1}^2}{s^2 + 2\zeta_1 w_{n1}s + \omega_{n1}^2} + \frac{K_{r2}\omega_{n2}^2}{s^2 + 2\zeta_2 w_{n2}s + \omega_{n2}^2} + \dots \quad (3.3)$$

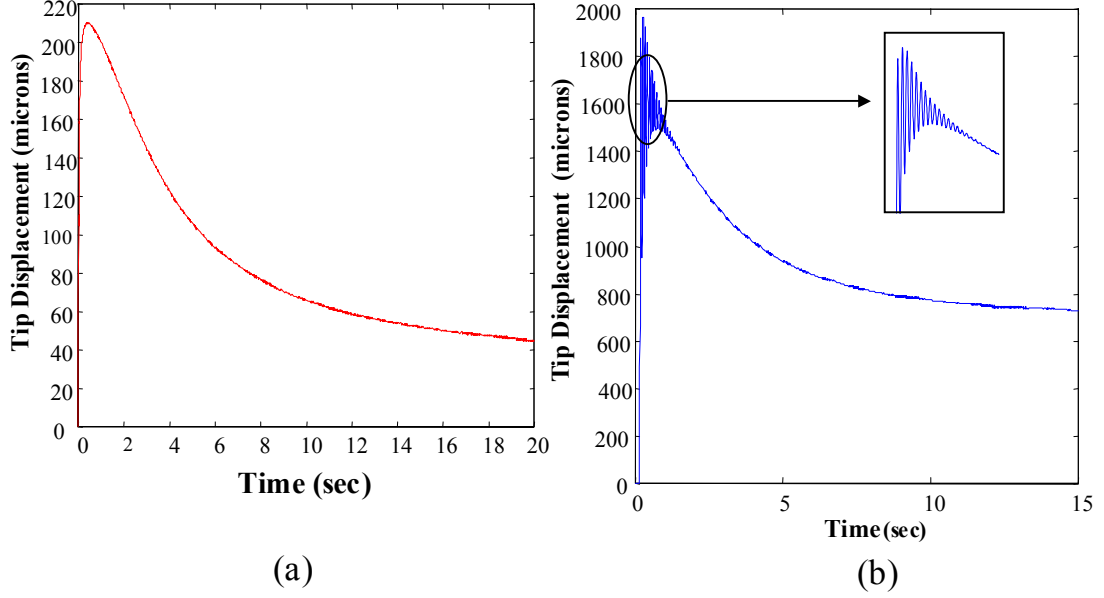


Figure 3.1: Bending response of (a) 12 mm x 5 mm x 0.2 mm actuator; (b) 40 mm x 5 mm x 0.2 mm actuator.

where ω_n is the natural frequency of the actuator, ζ is the nondimensional damping ratio, and K_r represents the gain coefficient of the resonant response. The accuracy of the empirical model might depend on the number of poles in the empirical model. A simpler model, with four linear poles and a single resonance term, of equation (3.3) can be written as,

$$G(s) = \frac{Y(s)}{U(s)} = \frac{a}{s + \alpha} + \frac{b}{s + \beta} + \frac{c}{s + \gamma} + \frac{d}{s + \delta} + \frac{K_r \omega_n^2}{s^2 + 2\zeta \omega_n s + \omega_n^2} \quad (3.4)$$

3.3.1 Optimization function: FMINCON

As in the previous work by Kanno, et al, we utilize a nonlinear least squares technique to find the optimal values of the actuator model. The optimization variables are the coefficients a, b, \dots , the time constants α, β, \dots , and the resonant parameter terms K_r, ω_n , and ζ . The optimization is constrained to guarantee that the steady-state displacement of the modelled response is equivalent to the measured response.

The MATLAB function FMINCON, Coleman and Zhang (2000) is used to find the solution to the optimization problem (Mathworks, 2000). The FMINCON function finds the constrained minimum of a scalar function of several variables starting at an initial

estimate. This is generally referred to as constrained nonlinear optimization or nonlinear programming. FMINCON finds the minimum of a constrained nonlinear multivariable function $f(x)$,

$$\begin{aligned} \min_x f(x) \quad & \text{subject to} \\ & c(x) \leq 0 \\ & ceq(x) = 0 \\ & A \cdot x \leq b \\ & Aeq \cdot x = beq \\ & lb \leq x \leq ub \end{aligned}$$

where x, b, beq, lb and ub are vectors, A and Aeq are matrices, $c(x)$ and $ceq(x)$ are functions that return vectors, and $f(x)$ is a function that returns a scalar. $f(x)$, $c(x)$ and $ceq(x)$ can be nonlinear functions.

Denoting the measured step response data $\tilde{y}(t_i)$, where t_i are the discrete sample times, the optimization problem is

$$\begin{aligned} \min \quad & \sum_{t_i} \left(\frac{y(t_i) - \tilde{y}(t_i)}{y(\infty)} \right)^2 \\ \text{subject to} \quad & \frac{A}{\alpha} + \frac{B}{\beta} + \dots + K_r = y(\infty) \\ & \alpha, \beta, \dots, \omega_n, \zeta > 0 \end{aligned} \tag{3.5}$$

where $y(\infty)$ is the steady state of the step response data.

For shorter polymers in which the resonant response is negligible, equation (3.5) is modified by setting $K_r = 0$ and eliminating the constraints on the natural frequency and damping ratio. The optimization routine results in the optimized variables which give the best fit of the experimental data.

3.3.2 Test Setup

A test setup is built to obtain the step response for a 1 Volt input, for the given ionic polymer material samples. The test setup consists of a set of two electrodes placed at the fixed end of the actuator. The sample is cantilevered from the electrodes and the displacement at approximately the tip of the actuator is measured with a laser vibrometer. The size of the

longer ionic polymer sample was 40 mm x 5 mm x 0.2 mm (unsupported length of 26.3 mm) and the size of the shorter ionic polymer was 12 mm x 5 mm x 0.2 mm (unsupported length of 5 mm). Five open-loop step responses are taken from each of the samples at different times. The samples are hydrated between the tests by boiling them in water for 30 minutes. The actuator is excited by a step voltage of 1V supplied by a power amplifier (50 V, 1.2 A) that is controlled by the signal from a digital signal processor (dSPACE, Inc. Model 1102). The digital signal processor measures the actuator displacement at the tip with the help of a Polytec OFV303 Sensor Head and OFV040 Scanning unit controlled by a Polytec OFV3001 Vibrometer Controller. The DSP also measures the voltage across the actuator, and the current through the actuator. Figure 3.2 is a schematic of the test setup.

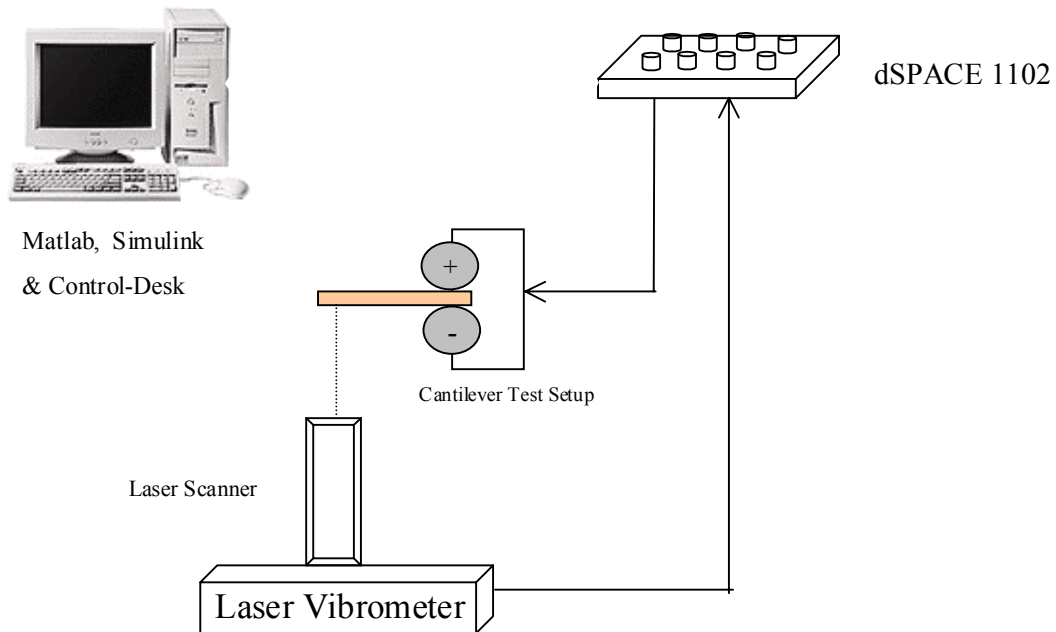


Figure 3.2: Experimental setup for the measurement of open-loop tip displacement for a 1V step input.

3.3.3 Optimized Results

The optimal curve fit obtained by the optimization routine and the experimental data for the short ionic polymer actuator using 3 real poles and no resonance term is shown in Figure 3.3a. The value of the cost function for this curve fit was 5.25. It is seen that the optimal curve fit of the data accurately matches the open-loop response curve of the shorter

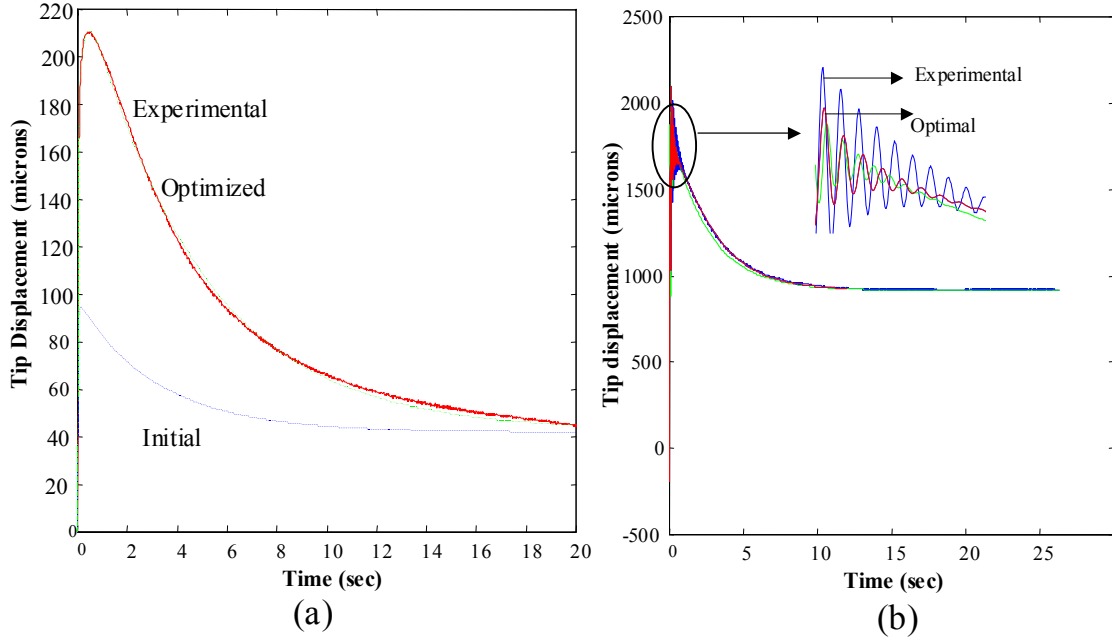


Figure 3.3: (a) Optimal curve fit using three real poles of the experimental data using for the 16 mm x 5 mm x 0.2 mm ionic polymer actuator sample to a 1 V step input; (b) Optimal curve fit using three real poles of the experimental data using for the 40 mm x 5 mm x 0.2 mm ionic polymer actuator sample to a 1 V step input.

polymer. The optimized transfer function for the short polymer using 3 real poles of one of the data set is shown in Equation 3.6. The optimized curve fit transfer function can be used to develop a control model for the shorter polymers.

$$G(s) = \frac{Y(s)}{U(s)} = \frac{-0.44}{s + 0.27} + \frac{802.39}{s + 69.88} + \frac{-957.21}{s + 108.87} \quad (3.6)$$

The optimal curve fit for one of the open loop response of the longer ionic polymer actuator using 3 real poles and one resonance term is shown in Figure 3.3b. The value of the cost function for this curve fit was 10.71. Figure 3.3b illustrates that the optimal curve fit of the data accurately matches the backbone of the open-loop response curve, but does not accurately match the resonances observed. This error of model might occur due to the FMINCON function optimization, which tries to reduce the summation of the error at each time step. The resonant portion of the response does not contribute substantially to the error cost function, therefore only minimal reductions in the cost function occur by matching the response in the first 2-3 seconds of the measurement. The optimized transfer function for the long polymer, using 3 real poles and one resonance term, of one of the data

set is shown in Equation 3.7.

$$G(s) = \frac{Y(s)}{U(s)} = \frac{10.31}{s + 13.08} + \frac{6.24}{s + 0.85} + \frac{-6.13}{s + 0.77} + \frac{0.71(75)^2}{s^2 + 2(0.09)(75) + (75)^2} \quad (3.7)$$

From the optimized results of the long polymer and the short polymer shown in this section, we can conclude that the simulation of the optimized transfer function model adequately match the step response data obtained from experiments. Hence, the transfer functions can be used to design a controller.

3.4 Cost Function Analysis

The curve fit obtained from the previous section shows the accuracy of the optimization routine in obtaining an empirical model. For a more rigorous analysis of the accuracy which can be obtained from this routine, a cost function analysis is done. The accuracy of the curve fit routine can be varied by varying the number of variables to be optimized. For example, the accuracy of the curve fit routine of an empirical model of long ionic polymer actuator will vary if the model includes two real poles and two resonance terms as opposed to a model consisting of three real poles and two resonance terms. Hence the need for a cost function analysis arises.

The optimization variables are the coefficients a , b , \dots , the time constants α , β , \dots , and the resonant parameter terms K_r , ω_n , and ζ . The number of variables can be altered, by increasing or decreasing the number of poles included in an empirical model. The accuracy of the empirical model might depend on the number of poles in the empirical model. The number of states in the control model is an important aspect of the design. Hence a study of the number of the real poles required to accurately model by optimization is performed by varying the number of real poles and considering one resonance term. A series of five open loop responses for the long polymer and short polymer are optimized for three different number of real poles in the system. The number of real poles is varied from 2 to 4. Here it is emphasized that the cost function is square of the error of the tip displacement of the experimental and simulated value normalized to the steady state value.

Table 3.1: Empirical model for short polymer using 2 real poles and one resonance term

Data Set	a	b	α	β	CF
1	-0.45	84.02	0.27	31.07	19.04
2	-0.46	69.36	0.34	29.10	6.34
3	-0.46	72.24	0.31	28.52	8.47
4	-0.47	56.19	0.33	23.17	6.47
5	-0.48	85.62	0.29	31.68	15.59

3.4.1 Short Polymer

The optimized parameters for the short polymer is presented in Table 3.1. Two real poles are used for modeling the short ionic polymer. It is seen from the table that each of the data set has one fast pole and one slow pole. For all the data sets, it is seen that, the poles are around the same region with similar gains. The optimized parameters for the short polymer using three real poles is illustrated in Table 3.2. Compared to the 2-pole model, the data set has two fast poles and one slow pole. The cost function for the data sets is less when compared to the cost function of the corresponding data set in Table 3.1.

Table 3.2: Empirical model for short polymer using 3 real poles and one resonance term

Data set	a	b	c	α	β	γ	CF
1	-0.44	802.39	-957.21	0.27	69.88	108.87	17.26
2	-0.44	408.766	-534.40	0.33	60.33	121.21	5.25
3	-0.45	421.1	-547	0.3	58.86	118.02	7.26
4	-0.466	286.57	-423.86	0.33	44.93	106.86	3.91
5	-0.5	886	-1046.9	0.288	72.38	109.6	13.79

Table 3.3 shows the optimized parameters of the four pole model for the ionic polymer actuator. The data set has three fast poles and one slow poles. On more closer observation by breaking the system into the zero-pole-gain format, it was seen that the optimization routine was placing additional zeros and poles closer to each other, effectively creating a pole-zero cancellation. For example, data set #1 in Table 3.3 has a transfer function shown in zero-pole-gain format in equation (3.8). The empirical model has a pole-zero cancellation at $s = -148$ approximately.

$$G(s) = \frac{Y(s)}{U(s)} = \frac{12247(s + 147.41)(s - 122.76)(s + 0.10)}{(s + 148.21)(s + 115.11)(s + 56.36)(s + 0.27)} \quad (3.8)$$

Table 3.3: Empirical model for short polymer using 4 real poles and one resonance term

Data set	a	b	c	d	α	β	γ	δ	CF
1	-0.44	358	-147.2	-352.67	0.27	56.36	115.11	148.21	17.314
2	-0.44	355	-148	-353.2	0.33	58.39	113.49	145.82	5.25
3	-0.45	355	-148	-353	0.3	56.6	113.06	145.09	7.26
4	-0.46	354	-139	-335	0.33	47.19	85.25	97	3.87
5	-0.47	359	-166	-375	0.28	58.104	147.9	158.2	13.83

For all the above three cases, on visual inspection it was seen that the simulated step response of the empirical model matched the experimental step response. The average cost function of the data sets for each case is presented in Table 3.4. The cost function represents the square of the error between the measured response and the model response normalized to the steady state value of the response. As shown in Table 3.4, increasing the number of real poles beyond 3 does not provide a substantial increase in model accuracy.

Table 3.4: Average cost function as number of real poles vary for short polymer

Number of real poles	Average Cost Function
2	11.182
3	9.49
4	9.4

3.4.2 Long Polymer

The long polymer is optimized using two real poles and a single resonance term, whose parameters are presented in Table 3.5. The data set has one fast pole and one slow pole. The damping coefficient is around 0.05. On visual inspection, the resonance data did not match very well in the the long polymers using the two pole model. The damping coefficient varies from 0.03 to 0.15 and the natural frequency varies around 72-80 rad/sec in the simulated empirical model.

Table 3.5: Empirical model for long polymer using 2 real poles and one resonance term

Data Set	a	b	α	β	Kr	ω_n	ζ	CF
1	22.21	-0.35	15.37	0.459	0.246	77.32	0.03	13.6
2	27.88	-0.45	17.25	0.28	0.96	78.56	0.05	10.17
3	11.66	-0.38	10.73	0.36	0.97	80.25	0.1	6.515
4	8.6	-0.38	9.76	0.34	1.24	72.47	0.13	8.435
5	5.07	-0.4	6.3	0.38	1.24	80.15	0.15	7.575

The optimized parameters for three real poles and a single resonance term for the longer polymer is presented in Table 3.6. Compared to the 2-pole model, the data set has one fast pole and two slow poles. Using the three pole model, the resonance data is matched better than the 2-pole model for the longer polymers on closer observation. The damping coefficient for each of the data set varies considerably whereas the natural frequency does not change substantially.

Table 3.6: Empirical model for long polymer using 3 real poles and one resonance term

Data set	a	b	c	α	β	γ	Kr	ω_n	ζ	CF
1	10.31	6.24	-6.13	13.08	0.85	0.77	0.71	75	0.09	10.71
2	14	-0.53	0	10.84	0.35	0.001	1.38	77.95	0.08	9.36
3	18.03	0.23	-0.05	14.56	0.83	0.39	0.75	81.2	0.07	5.63
4	2.09	-0.01	-0.44	4.54	0.10	0.413	1.72	66.41	0.48	6.7
5	0.877	-0.74	0.28	2.1	0.42	0.45	1.71	74.27	0.74	5.63

Table 3.7 shows the optimized parameters for four real poles and a single resonance term included in the transfer function. The data set has two fast poles and two slow poles. The resonance response of the polymer is matched better than the other two cases. The damping coefficient of the polymer in all the data sets is around 0.15 and the natural frequency is around 75 rad/sec. The change in the average cost function is presented in Table 3.8. As shown in Table 3.8, increasing the number of real poles beyond 3 does not provide a substantial increase in model accuracy.

Table 3.7: Empirical model for long polymer using 4 real poles and one resonance term

Data set	a	b	c	d	α	β	γ	δ
1	4.09	2.1	0.44	-2.46	8.28	0.92	0.91	0.73
2	560.76	-0.42	2442.67	-2806	48.16	0.28	144.72	99.34
3	-143.66	-0.35	-748	94.21	60.8	0.3	2584	28
4	48	-0.37	-25274	-64.3	22.5	0.34	49823	84
5	77.3	-0.6	0.28	42.8	31.6	0.4	0.653	75.62

Data set	Kr	ω_n	ζ	CF
1	1.01	71.6	0.20	12.24
2	2.29	77.73	0.12	6.83
3	1.3	80	0.12	5.60
4	1.25	73.83	0.11	6.34
5	1.22	74.21	0.13	4.42

Table 3.8: Average cost function as number of real poles vary for longer polymer

Number of real poles	Average Cost Function
2	9.07
3	8.1
4	7.75

3.4.3 Conclusions about the Cost Analysis

Cost function analysis was done for the shorter polymer and the longer polymer using one resonance term and varying the number of real poles to model the system from 2 to 4. As the number of real poles were increased in the short polymer model, there was no substantial increase in accuracy when observed visually. In the longer polymer, as the number of poles was increased, the resonance part of the response was modeled more accurately. It was also seen that as the number of poles increased in the short polymer and the long polymer, a pole-zero cancellation was propagating through the optimization method. Hence, by increasing the number of real poles in the ionic polymer model, a pole zero cancellation appears instead of an substantial increase in the accuracy. The pole-zero cancellation effect observed, results in an unstable system with a stable transfer function [Friedland (1986)]. The transfer function is of lower order than the system and the unstable modes are either

not capable of being affected by the input or not visible in the output, i.e. not completely observable and not completely controllable, which was proved by R.E. Kalman in 1950s. This unrealistic increase of poles increases the complexity of the controller design. The cost function analysis presented is one of the methods to prevent such effects to creep into the empirical model.

Figure 3.4a shows the cost function variation for each of the data set optimized in a short polymer, while Figure 3.4b shows the variation for the long polymer. It is seen that the cost function saturates as the number of real poles is increased from 3 to 4.

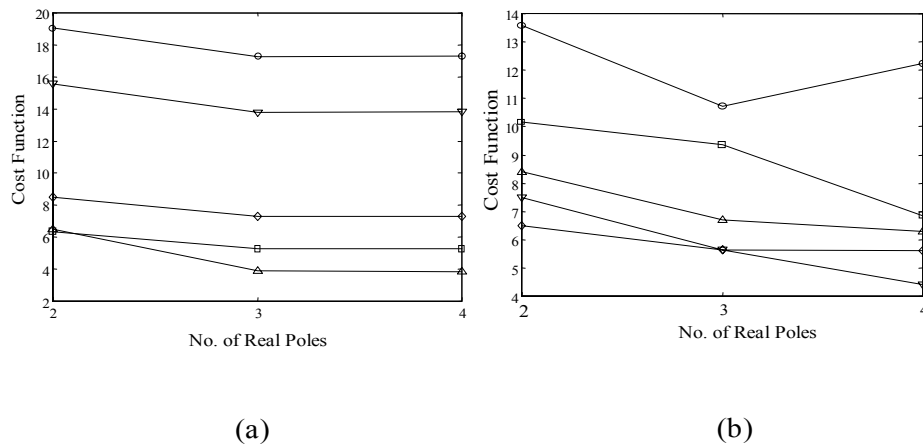


Figure 3.4: (a) Cost function variation for short polymers as number of real poles vary; (b) Cost function variation for long polymers as number of real poles vary.

3.5 Summary

An empirical model does not consider any physical phenomenon. In this chapter, an empirical model developed by Kanno et al. (1994) was modified to incorporate resonance behavior observed in longer polymers and was generalized for any length of ionic polymer. Short polymers with an unsupported length of 7.8 mm do not exhibit any resonance in the step response, hence they are modeled using 3 real poles. Longer polymers which exhibit resonance, are modeled using 3 real poles and 2 resonant poles. This empirical model was optimized using a function in MATLAB. The optimization results are analysed with respect to a cost function as the number of real poles was varied for short and long polymers.

The accuracy of the model can be changed by varying the number of poles in the model. A study of the cost function as the number of real poles are varied is done. It is seen that as the number of real poles is varied from 3 to 4, the cost function has no substantial decrement. Hence the empirical model developed using 3 real poles, can be used as a control model for the ionic polymer actuator.

In this chapter, the empirical model for the ionic polymer actuator is developed and optimized. This model can now be used for the design of a controller to increase the bandwidth of the actuator.

Chapter 4

Feedback Control

The dynamic response of the ionic polymer actuator illustrates a slow settling time and a high overshoot of the tip displacement when a step input voltage is applied. The ionic polymer actuator has a low bandwidth due to the slow settling time observed and cannot be used to actuate high frequency signals. Feedback control of the ionic polymer is necessary to overcome these disadvantages.

In this chapter, the optimized transfer function from the empirical model developed in the previous chapter is converted into a canonical state space model. A feedback controller is designed using the Linear Quadratic Regulator (LQR) method to increase the bandwidth of the ionic polymer actuator. Two methods of designing control systems using different cost functions in the LQR technique are discussed for long polymers. Simulations are performed on the closed-loop system which indicate faster settling time and a reduction in overshoot. A perturbation analysis is discussed on the effect of the change in natural frequency on the closed-loop stability of the system.

4.1 State Space Model

A state space model represents the dynamics of a system by a number of first-order differential equations. The optimized transfer function [Eq. (3.6) & Eq. (3.7)] is converted into a canonical state space representation. The ionic polymer actuator is represented as a parallel interconnection of subsystems which is advantageous for the control design. Although the input-output relationship is independent of the state variable representation, representing the dynamics in this form allows us to directly relate the states to the time constants of

the response. This is a necessary step for the LQR control used in the feedback which is discussed in the next section.

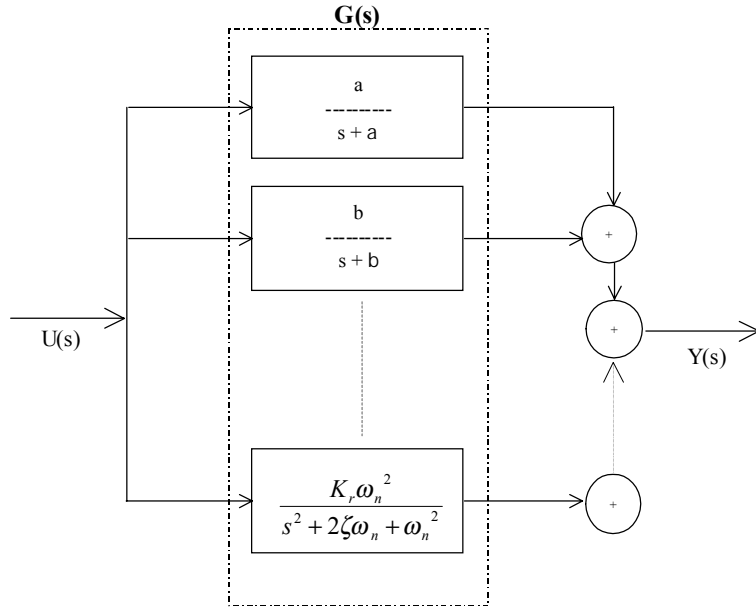


Figure 4.1: Parallel interconnection of the control model.

The optimal values of the parameters determined from the empirical model optimization are substituted into the transfer function as given by equation (3.4). A canonical state space model of the form

$$\begin{aligned} \dot{x}(t) &= Ax(t) + Bu(t) \\ y(t) &= Cx(t) + Du(t) \end{aligned} \tag{4.1}$$

is obtained from the optimized transfer function, where $x(t)$ is the state vector, $u(t)$ is the control input, $y(t)$ is the output (tip displacement) of the system and A, B, C, and D are the state matrices. The system transfer function is treated as a parallel interconnection of smaller systems as shown in Figure 4.1. Assuming this structure, equation (4.1) has the form

$$\dot{x}(t) = \begin{bmatrix} -\alpha & 0 & \dots & 0 & 0 \\ 0 & -\beta & \dots & 0 & 0 \\ 0 & 0 & \ddots & 0 & 0 \\ 0 & 0 & 0 & 0 & 1 \\ 0 & 0 & 0 & -\omega_n^2 & -2\zeta\omega_n \end{bmatrix} x(t) + \begin{bmatrix} a \\ b \\ \vdots \\ 0 \\ K_r\omega_n^2 \end{bmatrix} u(t)$$

$$y(t) = \begin{bmatrix} 1 & 1 & \dots & 1 & 0 \end{bmatrix} x(t) \quad (4.2)$$

The effect of the parallel system interconnection shows up in the matrix A, wherein, the smaller systems show up as states corresponding to the diagonal elements, and the resonance corresponds to the coupled set of elements in the last two rows of the matrix A. The change in first elastic resonance as the ionic polymer actuator hydrated and dehydrated was discussed in Section 2.3.2. This change can be modeled as the natural frequency (ω_n) multiplied by a perturbation (Δ). The state space model which includes perturbation term is shown in Equation 4.3.

$$\dot{x}(t) = \begin{bmatrix} -\alpha & 0 & \dots & 0 & 0 \\ 0 & -\beta & \dots & 0 & 0 \\ 0 & 0 & \ddots & 0 & 0 \\ 0 & 0 & 0 & 0 & 1 \\ 0 & 0 & 0 & -[\omega_n(1 + \Delta)]^2 & -2\zeta\omega_n(1 + \Delta) \end{bmatrix} x(t) + \begin{bmatrix} a \\ b \\ \vdots \\ 0 \\ K_r[\omega_n(1 + \Delta)]^2 \end{bmatrix} u(t)$$

$$y(t) = \begin{bmatrix} 1 & 1 & \dots & 1 & 0 \end{bmatrix} x(t) \quad (4.3)$$

The compensator is designed using LQR technique in two ways utilizing two different cost functions as explained in Section 4.2. After the compensator has been designed, an analysis of performance and stability of the closed-loop system as resonance perturbation is introduced is necessary to select the right cost function. Equation 4.3 will be used as model for this analysis.

The state space model is checked for controllability and observability. It is clear from Figure 4.1 that the control input influences all of the states in the model, and that all of the states influence the output. Thus, the system is both controllable and observable

indicating that the closed-loop poles can be placed anywhere in the complex plane using full-state feedback and a linear observer.

4.2 Design of Controller

4.2.1 Linear Quadratic Regulator(LQR) Control

State-space control approaches are used to design feedback control laws for the ionic polymer actuators using a model that consists of three real poles. Two additional resonance states are used to model the actuator resonance for the longer polymer. To control the system, the states are estimated by designing a linear observer-estimator as shown in Figure 4.2.

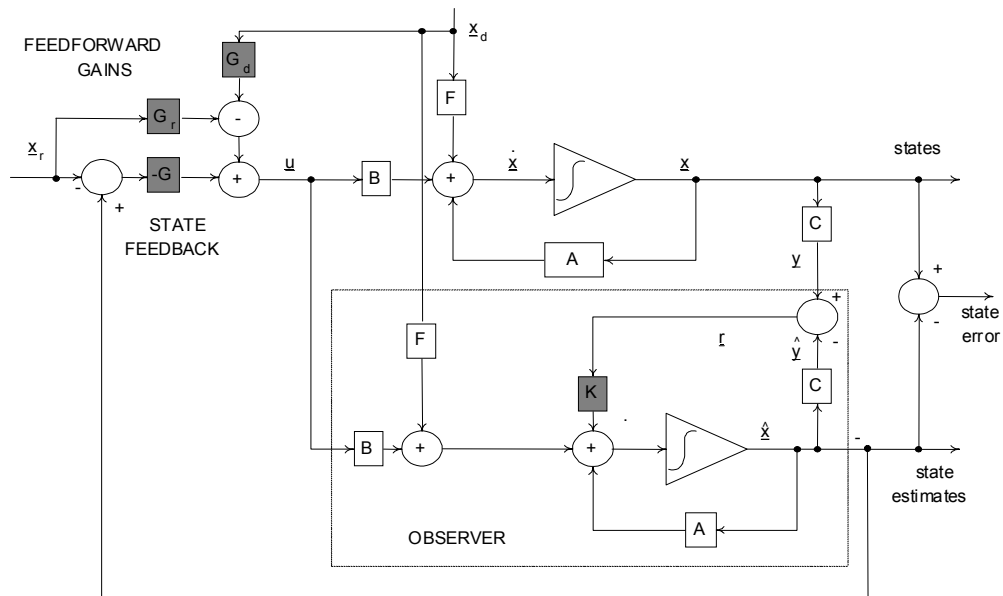


Figure 4.2: Linear Observer-Estimator compensator to track reference inputs in state space design.

For the design of the controller, we will utilize Linear Quadratic Regulator (LQR) control theory to determine a set of state feedback gains. The LQR optimization produces an optimal full-state feedback gain matrix G . It is well known that LQR control can be used for optimizing the performance with respect to a quadratic cost function [Friedland (1986)]. The cost function is comprised of a quadratic function of the states and a quadratic

function of the control input,

$$V = \int_0^{\infty} [x'(t) Q(t) x(t) + u'(t) R(t) u(t)] dt \quad (4.4)$$

The design parameters are the state weighing matrix Q and control weighting matrix R . The Q matrix is to be chosen in such a way that its influence can be studied on the output. We will study two control cases.

Case 1 : In the first case, the weighting matrices are chosen as

$$Q = C' C \quad R = \frac{1}{r} \quad (4.5)$$

Substituting equation (4.5) into equation (4.4), we obtain

$$\begin{aligned} V &= \int_0^{\infty} \left[x'(t) C' C(t) x(t) + u'(t) \frac{1}{r}(t) u(t) \right] dt \\ V &= \int_0^{\infty} \left[y(t)' y(t) + u'(t) \frac{1}{r}(t) u(t) \right] dt \\ V &= \int_0^{\infty} y^2(t) + \frac{1}{r} u^2(t) dt \end{aligned} \quad (4.6)$$

We see that the optimal controller will minimize the output and that the only design parameter is the scalar r . Increasing r will reduce the influence of the control on the cost function.

Case 2 : The second control case utilizes weighting matrices of the form

$$Q = C'_m C_m \quad R = \frac{1}{r} \quad (4.7)$$

where

$$C_m = \begin{bmatrix} 1 & 1 & 1 & 0 & 0 \end{bmatrix} \quad (4.8)$$

In this case the cost function reduces to

$$V = \int_0^{\infty} x_1^2(t) + x_2^2(t) + x_3^2(t) + \frac{1}{r} u^2(t) dt \quad (4.9)$$

4.2.2 Linear Observer-Estimator

The external inputs, reference input (x_r) and disturbance input (x_d) are fed in to the system through feedforward gains G_r , G_d and F . However, in this work no disturbance input is

considered. Hence, $x_d = 0$ & $F = G_d = 0$. The poles due to full-state feedback are the eigenvalues of the matrix $A - BG$. The rate of convergence of the estimated states to the actual states is controlled by choosing the observer gain matrix K . The gain matrix K is chosen by pole placement method by specifying the eigen values of the observer state matrix $A - BK$. The eigenvalues of the observer state matrix $A - KC$ are chosen to be a multiple of two of the full-state feedback poles. This selection keeps the control gains low and thereby maintains the control voltage across the polymer within acceptable limits while ensuring that the observer error will converge to zero in an acceptable amount of time.

The final component of the control design is to compute a feed forward gain matrix G_r that eliminates steady-state error. G_r is chosen to eliminate the steady state output error due to the reference input and is computed as shown in Equation[4.10]. Further details of this computation are provided in Friedland (1986).

$$G_r = \left[C (A - BG)^{-1} B \right]^{-1} C (A - BG)^{-1} E \quad (4.10)$$

where

$$E = \left[(A - A_r) \quad F \right]$$

Since, for a step input $A_r = 0$, we have $E = A$. Substituting the value of E in Equation[4.10], we have

$$G_r = \left[C (A - BG)^{-1} B \right]^{-1} C (A - BG)^{-1} A \quad (4.11)$$

After computing the observer gain matrix K and feed forward gain G_r , the state space model for the observer-estimator compensator is,

$$\begin{aligned} \hat{x}'(t) &= [A - BG - KC] \hat{x}(t) + \begin{bmatrix} BG - BG_r & K \end{bmatrix} \begin{bmatrix} x_r(t) \\ y(t) \end{bmatrix} \\ u(t) &= [-G] \hat{x}(t) + \begin{bmatrix} G - G_r & 0 \end{bmatrix} \begin{bmatrix} x_r(t) \\ y(t) \end{bmatrix} \end{aligned} \quad (4.12)$$

where $\hat{x}(t)$ is the state estimate vector, $x_r(t)$ is the reference input vector and $y(t)$ is the output (tip displacement) of the system. Simulations of the closed-loop system are obtained

by substituting $u = -G\hat{x}$ into equation (4.1) and equation (4.12) and combining them into one matrix expression for the closed-loop system shown in Equation[4.13].

$$\begin{aligned} \begin{Bmatrix} \dot{x}(t) \\ \dot{\hat{x}}(t) \end{Bmatrix} &= \begin{bmatrix} A & -BG \\ KC & A - KC - BG \end{bmatrix} \begin{Bmatrix} x(t) \\ \hat{x}(t) \end{Bmatrix} + \begin{bmatrix} BG - BG_r \\ BG - BG_r \end{bmatrix} \{x_r(t)\} \\ y(t) &= \begin{bmatrix} C & 0 \end{bmatrix} \begin{Bmatrix} x(t) \\ \hat{x}(t) \end{Bmatrix} + 0 \{x_r(t)\} \end{aligned} \quad (4.13)$$

To study the influence of the cost function on resonance suppression in the closed-loop system, the control designs for the longer polymers will be simulated using both the above cases of weighting matrices. For the shorter polymers, oscillations due to resonance are not present. Hence the cost function used in Case 1 will be used to design the compensator for short polymers.

4.3 Closed-loop Control Simulation

Simulations with both the choices of the Q matrix are performed for various optimized models. The objectives of the controller design are

1. To achieve a faster settling time compared to the open loop,
2. To reduce overshoot,
3. To keep the control voltage across the polymer to less than 3 Volts to prevent electrolysis or any damage to the ionic polymer actuator.

The control design is now a function of the scalar parameter, r . Increasing r gives less weight to the control effort and should effect a reduction in the settling time, and decreasing r gives less weight to the limit of control voltage on settling time.

4.3.1 Short polymer

Simulations for various values of the control design parameter r are shown in Figure 4.3 and Figure 4.4 for the short polymer actuator (7.8 mm x 5 mm x 0.2 mm). Figure 4.3 illustrates that increasing r reduces the overshoot of the step response of the tip displacement and decreases the time required for the actuator to reach a steady-state value. The achievable

settling time is limited by the maximum control input objective. High values of r exhibit a faster settling time, but increases the gains leading to an increase in initial control input. Figure 4.4 illustrates the control input required to the polymer as a function of r .

The simulations indicate that the closed-loop control signal consists of a large initial input followed by a slow increase in the voltage to a steady-state value. We hypothesize that the slow voltage increase is required to offset the relaxation of the polymer. Kanno et al. (1996b) and Newbury and Leo (2001) has measured the current variation for a step input of a open-loop ionic polymer actuator which shows the capacitive nature of the actuator. For a capacitor, the rate of change of voltage is proportional to the current flowing in the capacitor. Due to the capacitive nature of the actuator, we believe that this slow voltage rise will have a constant gradient and hence will result in a constant current across the polymer.

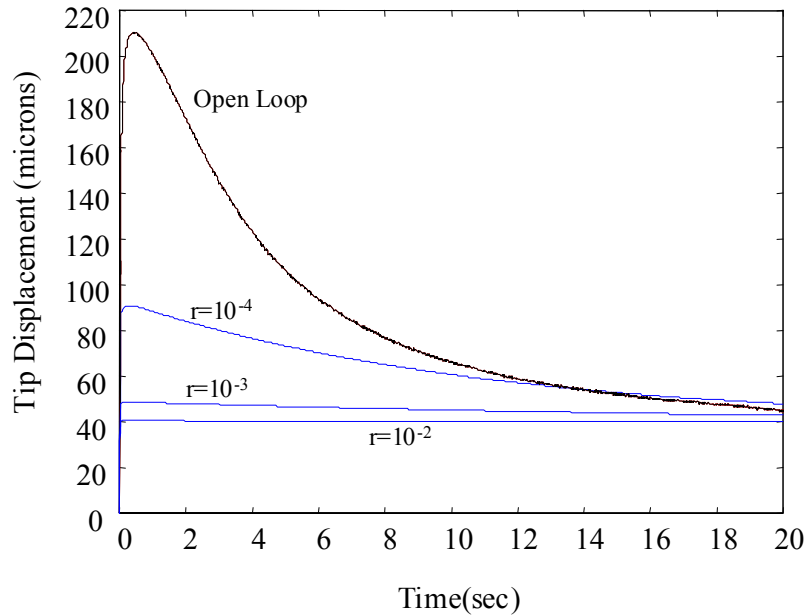


Figure 4.3: Simulation of closed-loop tip displacement of the 7.8 mm-long polymer for varying values of the control design parameter r .

The control simulations demonstrate that the response time of the actuator can be significantly increased with feedback control. The large overshoot and slow relaxation of the actuator is eliminated by feedback control that utilizes tip displacement as the sensor signal and voltage as the control signal. Table 4.1 shows the trade-off between maximum control input and settling time as a function of the design parameter r . The simulations

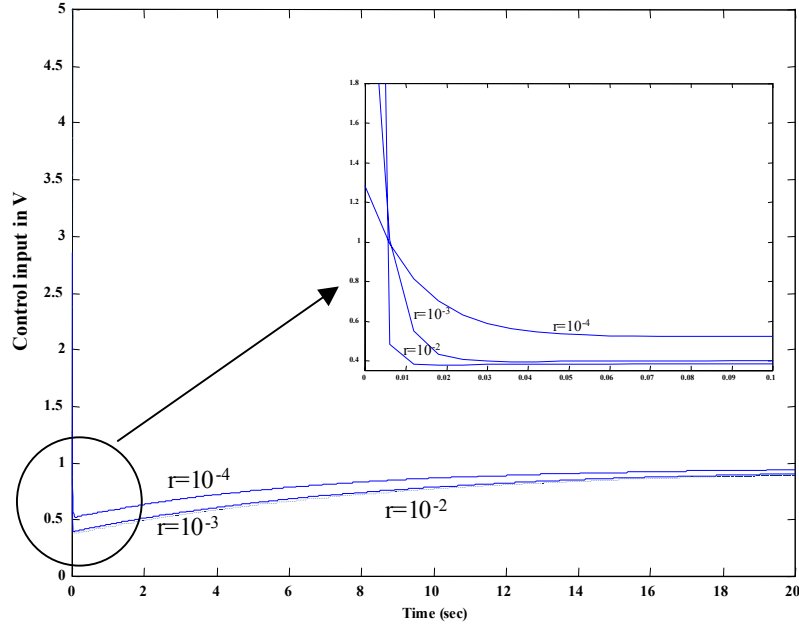


Figure 4.4: Simulation of the control input of the 7.8 mm-long polymer for varying values of the control design parameter r .

demonstrate that the settling time can be decreased by more than 80% using LQR control.

Table 4.1: Trade-off between peak control input & settling time.

r	Settling time(sec)	Peak control input(Volts)
10^{-4}	12	0.8
10^{-3}	6	2.2
10^{-2}	1	3.8

The placement of the closed-loop poles selected by the LQR is shown in a represented root locus plot in Figure 4.5. The optimal controller selects closed loop poles for a third order system. One of them is placed very near to the zero close to the origin which leads to a near pole-zero cancellation. The cancellation of the open-loop zero decreases the overshoot of the system and leads to a lower order system which responds faster to the given step input. The other two poles are placed to the left of the origin as well as the open loop pole leading to faster settling time. This placement of the poles is the best way for LQR to nullify the effects of the slower dynamics of IPMC and obtain a faster response time.

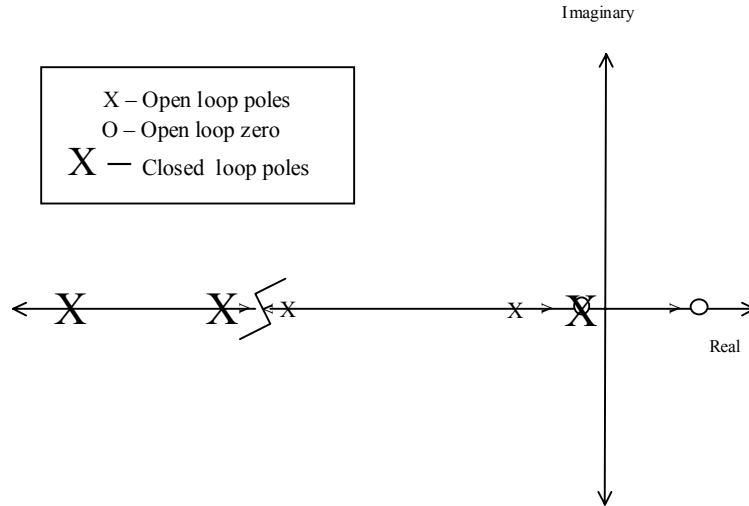


Figure 4.5: Root Locus representation of the closed-loop system of the short polymer.

It is well known from nyquist stability theory that the stability of the closed-loop system can be analysed by studying open loop series transfer function of the plant multiplied by compensator transfer function (loop transfer function). Figure 4.6 shows the bode plot of loop transfer function of the short ionic polymer actuator. The system is very stable indicated by a phase margin of 86° at 37.64 Hz (233.6 rad/sec), an infinite gain margin and a bandwidth of 63.66 Hz (400 rad/sec).

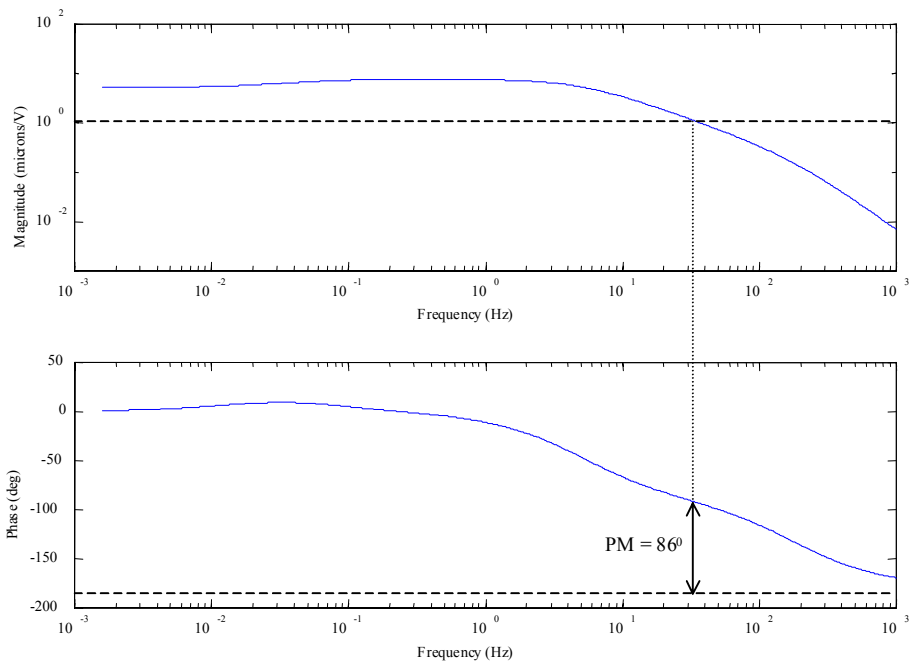


Figure 4.6: Bode plot of the closed loop system of the short polymer.

4.3.2 Case 1: Long polymer - Resonance term included in Q

A second series of control simulations are performed for the model of the 26.3 mm-long ionic polymer actuator using a control design that incorporates the resonance terms in the LQR cost function (i.e. $Q = C'C$). Figure 4.7 illustrates that control system provides reduction of the settling time as the r factor is increased. The reduction in settling time is accompanied by a decrease in the oscillatory response of the polymer in the first 2-3 seconds of the step response. The control input for the simulation cases are shown in Figure 4.8. The control signal for this case has the same characteristics as the control signal for the short polymer (Figure 4.4), but exhibits a oscillatory response in the first 2 seconds to nullify the effects of the resonance (see the inset of Figure 4.8).

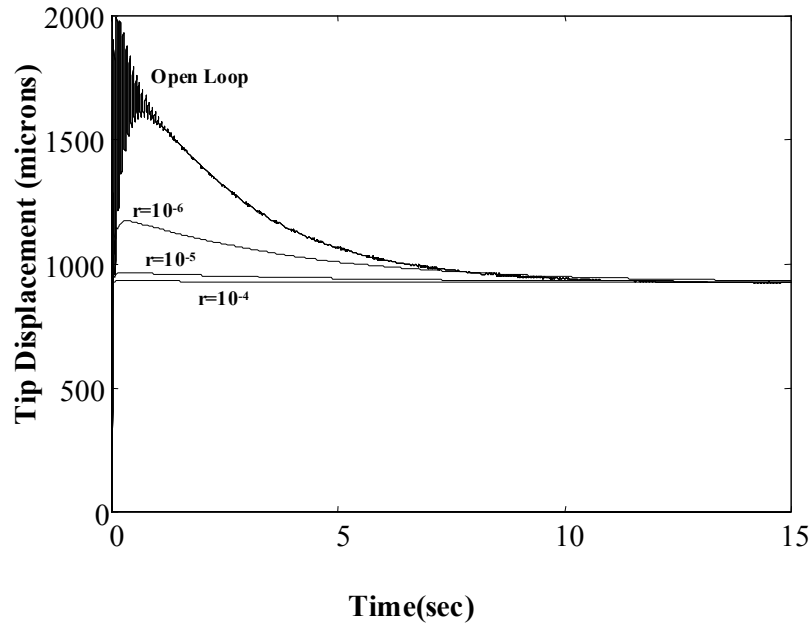


Figure 4.7: Simulation of the tip displacement for the 26.3 mm long polymer with weighting matrix $Q = C'C$.

The low frequency oscillations seen in the open-loop data of the step response are now reduced considerably by using the controller in the closed-loop system. Hence, time response simulations indicate that feedback control is eliminating the effects of resonance in the response of the polymer actuator. This is investigated in more detail by examining the frequency response functions of the plant, compensator, and the system defined by the series combination of the plant and compensator. Figure 4.9a is the frequency response of

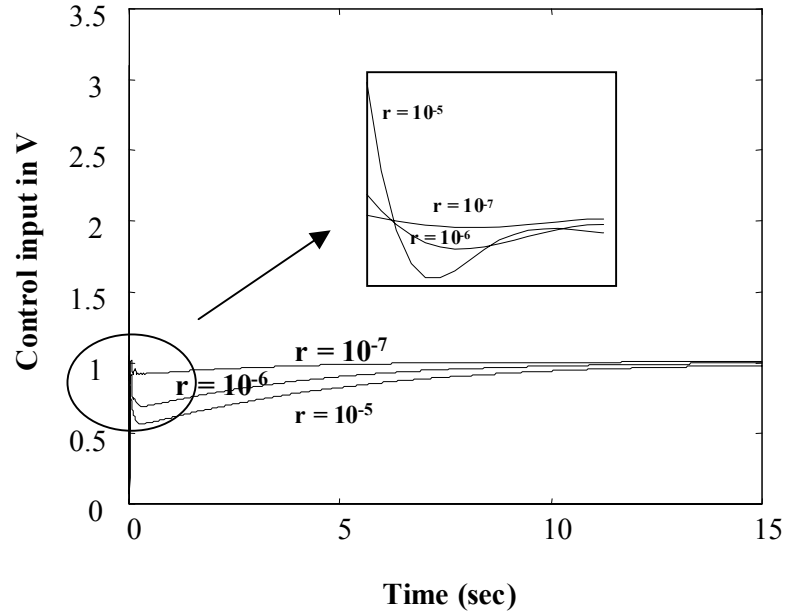


Figure 4.8: Simulation of the control input for the 26.3 mm long polymer with weighting matrix $Q = C'C$.

the plant illustrating the low frequency dynamics associated with the time constants α , β , and γ , and the magnitude and phase changes associated with the resonant terms in the 10-20 Hz frequency range. The resonant frequency is approximately at 13 Hz for this actuator at the time of experiment. Figure 4.9b is the bode plot of the compensator and the system, which illustrates that the LQR controller is a lead compensator that adds phase near the resonance frequency of the actuator. Lead compensation increases the phase margin and provides closed-loop damping to the actuator resonance.

Examining the closed loop poles selected by the LQR, we see a very interesting result. The optimal controller selects closed loop poles for a fifth order system, as shown in Figure 4.10. Three of them are placed near to the zeros which leads to a near pole-zero cancellation. The cancellation of the open-loop zero decreases the overshoot of the system and makes the response faster to the step input. The set of resonance poles are placed diagonally far from the open loop resonance poles to the left of the s-plane leading to faster settling time. Hence the closed-loop resonance poles are placed at a higher damping ratio than the open-loop resonance poles, increasing the settling time. LQR minimizes the effect of resonance in the longer polymers and leads to a faster settling time with less overshoot with this placement of the poles. Figure 4.11 shows the bode plot of the series connection of

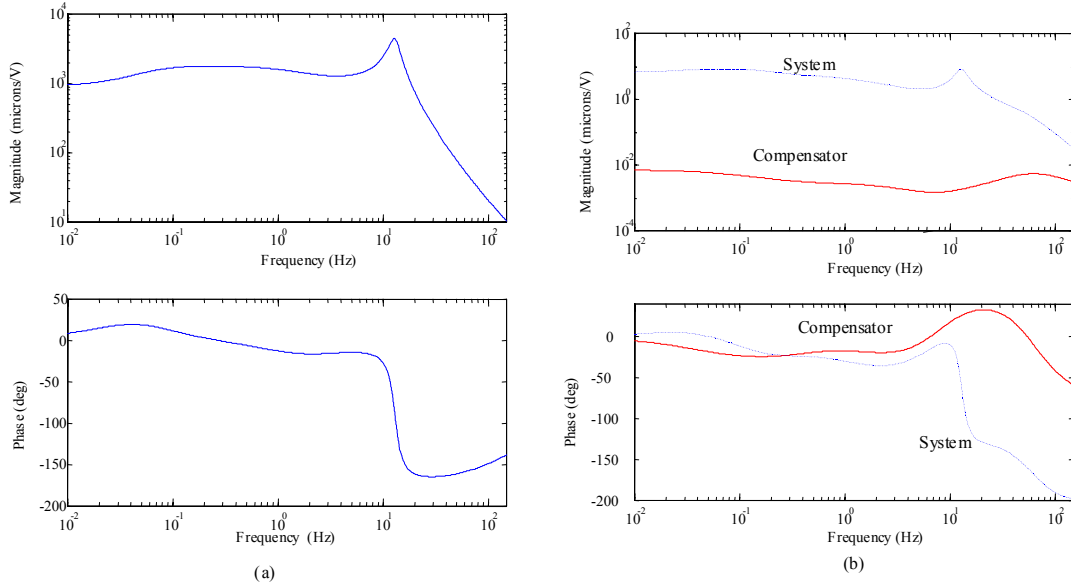


Figure 4.9: (a) Transfer function of the actuator at the time of the experiment; (b) Bode plot of the compensator and the system for $Q = C'C$.

actuator and compensator of long ionic polymer actuator for Case 1. The system is stable and gives satisfactory performance which is indicated by a phase margin of 46° at 27.5 Hz (174 rad/sec), a high gain margin of 15.7 dB at 80 Hz (498 rad/sec) and a bandwidth of 33.42 Hz (210 rad/sec).

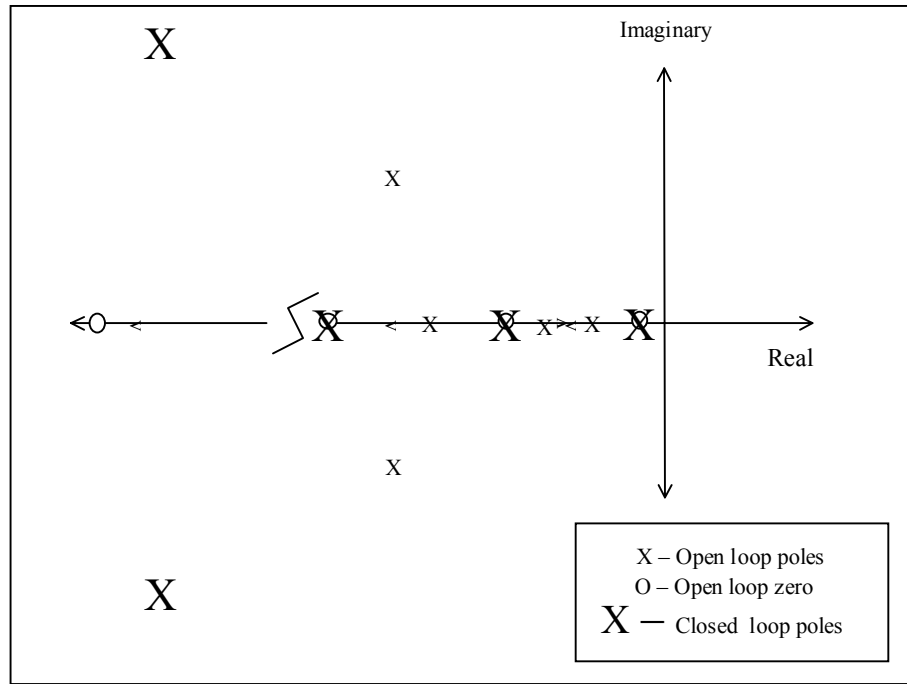


Figure 4.10: Root Locus representation of the closed-loop system of the long polymer for Case 1.

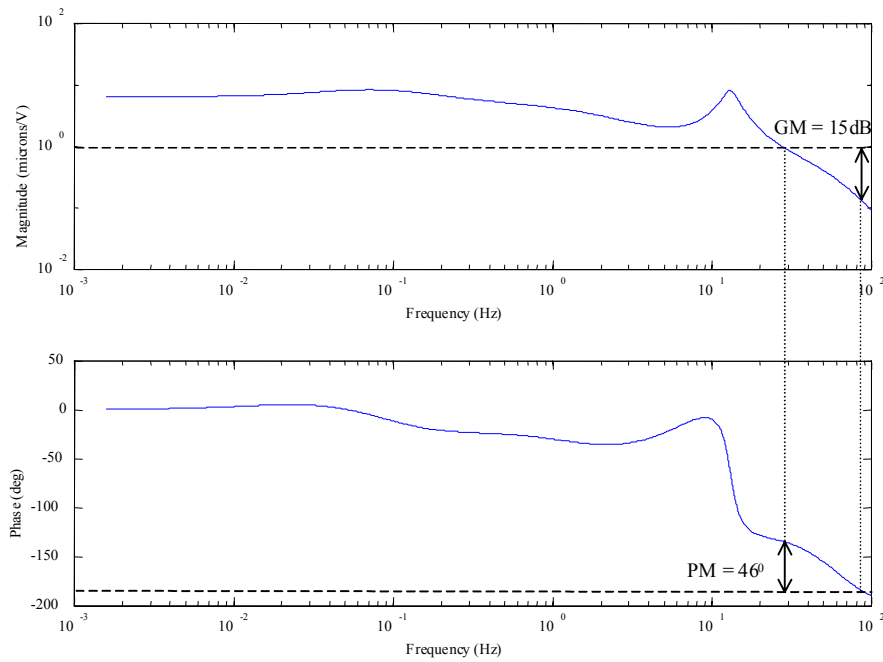


Figure 4.11: Bode plot of the series plant and compensator of the long polymer for Case 1.

4.3.3 Case 2: Long Polymer - Resonance term ignored in Q

A final series of control simulations are performed using the weighting matrix $Q = C_m' C_m$. Figure 4.12a shows a change in the settling time as the r factor is increased. The primary difference between the controlled response for this weighting matrix and the weighting matrix for Case 1 is that the closed-loop response still exhibits oscillation in the first 2-3 seconds after the step is applied. Figure 4.12b shows the increase in the control input as the r factor is increased. The rationale for this time response is examined by investigating the frequency response of the compensator and system. Figures 4.13a and b are the Bode plots for the plant, compensator, and system. Figure 4.13b illustrates that the compensator is adding a notch at the resonant frequency of the plant. The settling time does not change as much as the previous case due to the rolloff at higher frequencies, but the notch in the compensator does not provide the phase lead as in the case of the design that utilized $Q = C' C$ as the state weighting matrix. Due to this, the bandwidth is limited and the controlled response still exhibits the oscillations associated with resonance of the actuator.

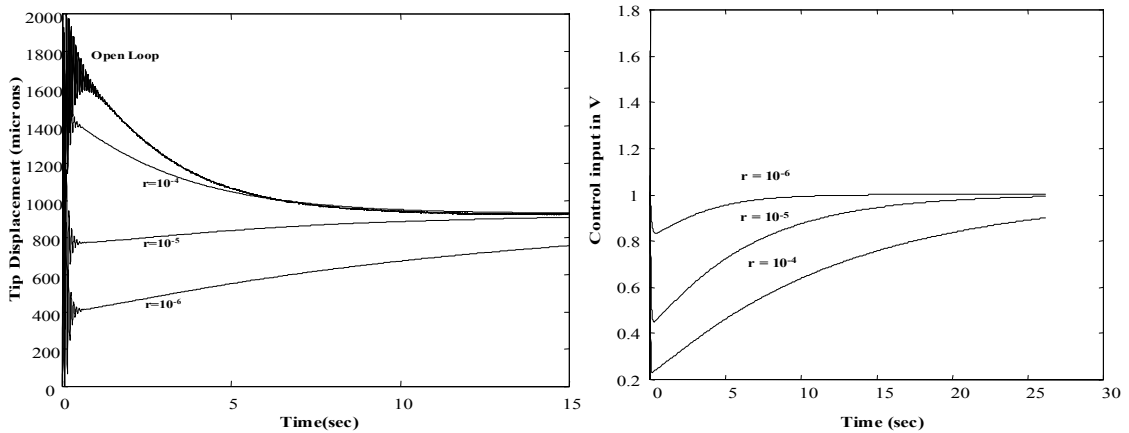


Figure 4.12: (a) Simulation of the tip displacement for the 40 mm-long polymer for $Q = C_m' C_m$; (b) Simulation of the control input.

In both the above cases, the slope of the control voltage input decreases as time progresses during settling. The reason for this behavior can be explained by the nature

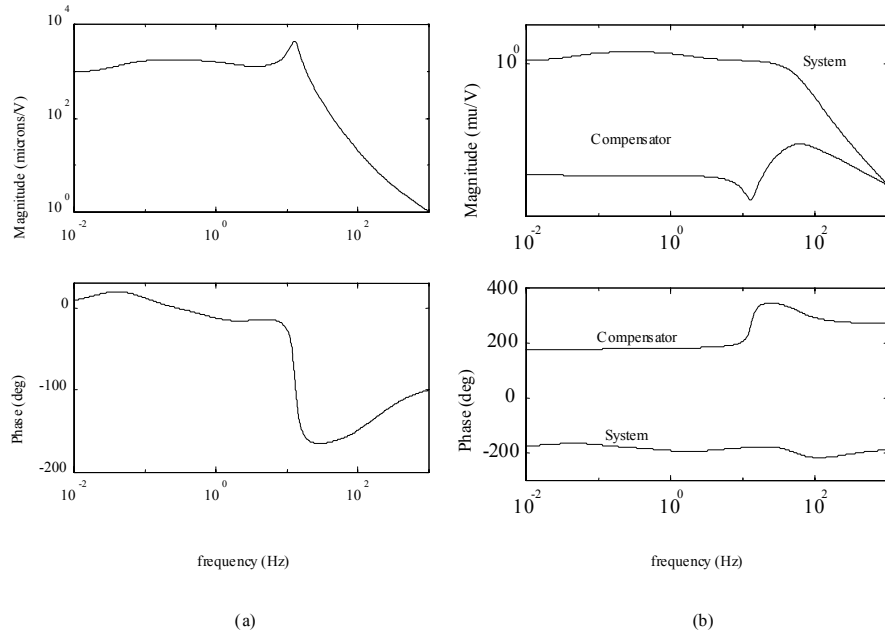


Figure 4.13: (a) Bode plot of the plant; (b) Bode plot of the compensator and system for $Q = C'_m C m$.

of the ionic polymer actuator to behave largely as a capacitor. In the absence of feedback control, the current through the actuator increases rapidly and then decreases exponentially to zero (Kanno, R., 1994) when a step voltage is applied. After this rapid increase, the current through the ionic polymer actuator does not decrease exponentially to zero as in the open loop. The control voltage has a gradual slope during the settling. This shows that current is still flowing through the ionic polymer actuator and its slope also varies until the control voltage is steady. Taking the physical phenomenon into account as predicted by plausible models suggested by others, we can deduce that the current is flowing across the polymer to oppose the back diffusion of the water in the ionic polymer actuator.

Examining the closed loop poles selected by the LQR, we see a classic example of pole-zero cancellation. As shown in Figure 4.14, the cancellation takes place at the four locations on the s-plane. The open-loop resonance poles are cancelled by placing a closed-loop zero. Two sets of pole-zero cancellation are introduced by the compensator at two locations on the real axis. Compared to the other cases, the open loop zero very close to the origin is not cancelled. Hence overshoot in the system and the response to the step input do not change adequately. A set of resonance poles are placed diagonally far from the open loop resonance poles to the left of the s-plane. Figure 4.15 shows the bode plot of

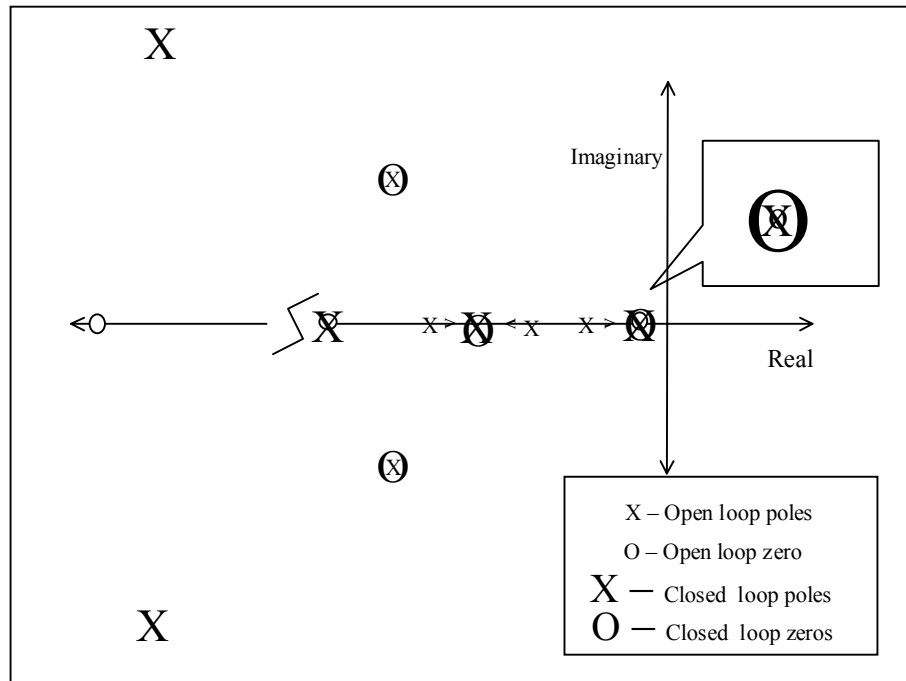


Figure 4.14: Root Locus representation of the closed-loop system of the long polymer for Case 2.

the series connection of actuator and compensator of long ionic polymer actuator for Case 2. The system is very close to being unstable. The bode plot illustrates the proximity to instability by a phase margin of 53.9° at 13.37 Hz (83.8 rad/sec), a very low gain margin of 4.3dB at 27.5 Hz (173 rad/sec).

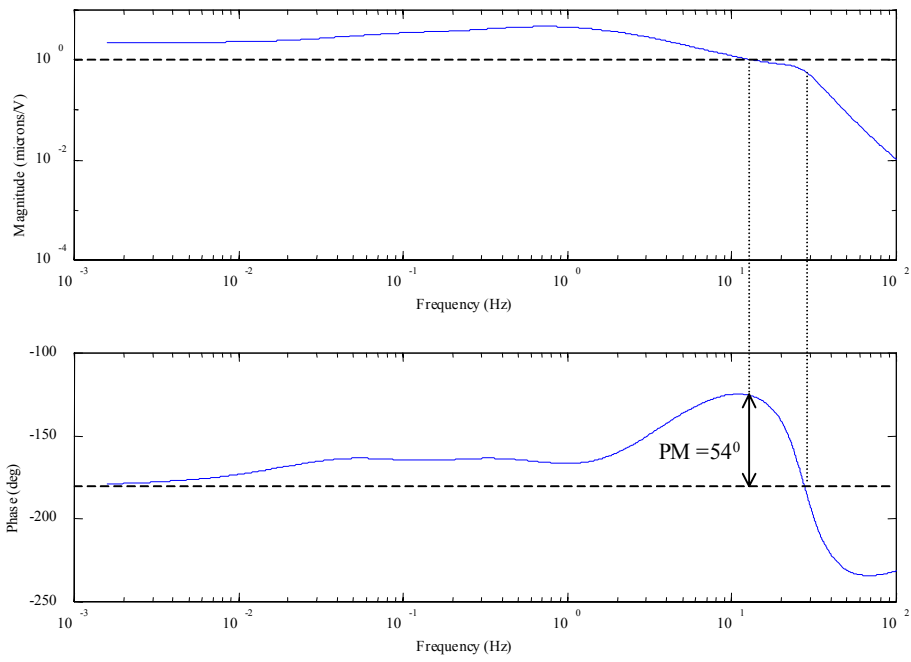


Figure 4.15: Bode plot of the series plant and compensator of the long polymer for Case 2.

4.3.4 Simulations with Perturbation

At the end of Section 4.1, perturbation variable (Δ) was introduced to model the changes in the natural frequency (ω_n) of the ionic polymer actuator. The stability of the closed-loop system of the long ionic polymer actuator is analyzed by simulating the system with perturbation for both of the above discussed cost functions.

Case 1: Resonance term included in Q

Figure 4.16 shows the simulation of the tip displacement for $r = 10^{-4}$ for a perturbation factor of 9%, in which the resonant frequency of the ionic polymer plant is changed from 13 Hz to 14.2 Hz. The settling time to steady state increases to 3.2 seconds as compared to the zero-perturbation settling time. The bode plot shown in Figure 4.17 illustrates that the phase margin of 42° does not change substantially from the zero perturbation phase margin of 46° and the gain margin still remains high. The stability of this system illustrates that the cost function used in the design of the compensator is robust for perturbation in the resonant frequency.

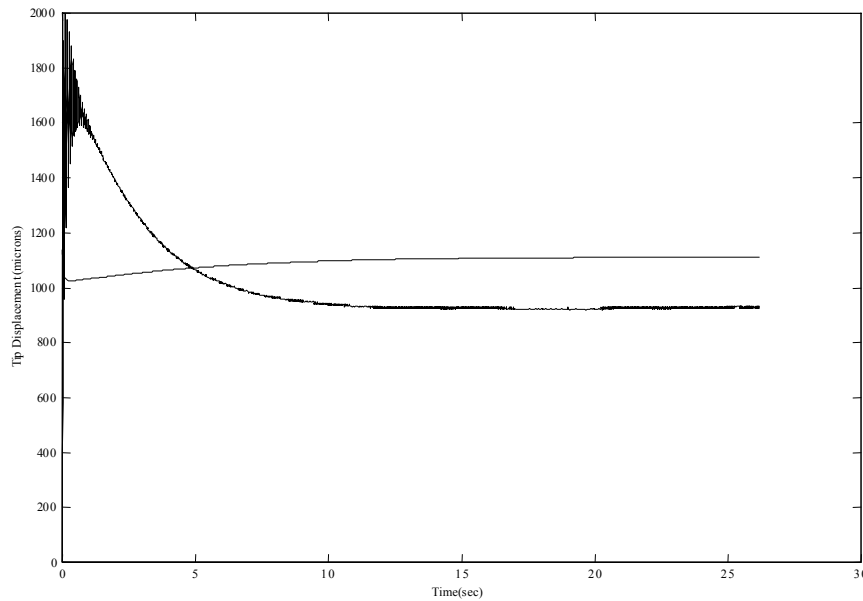


Figure 4.16: Tip displacement of the long polymer actuator for a perturbation factor of 9% in Case 1.

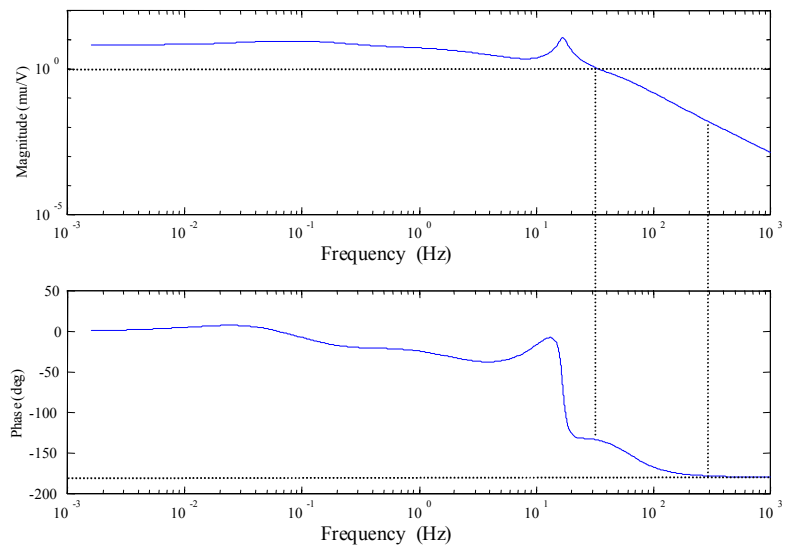


Figure 4.17: Bode plot of the series plant and compensator of the long polymer for a perturbation factor of 9% in Case 1.

Case 2: Resonance term not included in Q

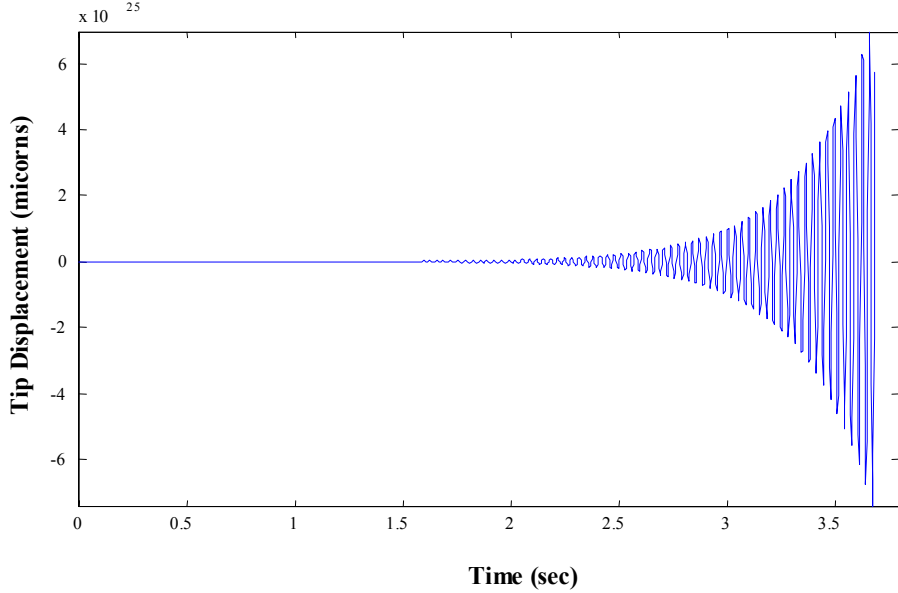


Figure 4.18: Tip displacement of the long polymer actuator for a perturbation factor of 9% for case 2.

Figure 4.18 shows the simulation of the tip displacement for $r = 10^{-4}$ for a perturbation factor of 9%, in which the resonant frequency changed from 12 Hz to 14 Hz. The system is unstable. The bode plot shown in Figure 4.19 illustrates that the closed-loop is unstable since the phase margin and the gain margin are zero. The proximity to instability in the system to a change in natural frequency of the plant by 9% proves that the cost function used for the design of the compensator is not preferred if perturbation in the resonant frequency occurs.

The variation of the ratio of the settling time with perturbation to the settling time without perturbation as the perturbation factor Δ varies, is shown in Figure 4.20. In case 1, The settling time of the polymer increases as $\Delta \rightarrow -0.3$. Similarly, the settling time also increases as $\Delta \rightarrow +0.3$. However, the system is stable for $-0.3 < \Delta < 0.3$ for case 1.

In contrast, in case 2, the settling time of the polymer does not change much as $\Delta \rightarrow -0.3$. This can be explained as the compensator has a low gain margin at lower frequencies. Hence, at the resonant frequency of the ionic polymer, the magnitude of the compensator times the plant is very low, which does not affect the stability of the system. However, the closed-loop system of the polymer goes unstable as $\Delta \rightarrow +0.3$. This is due

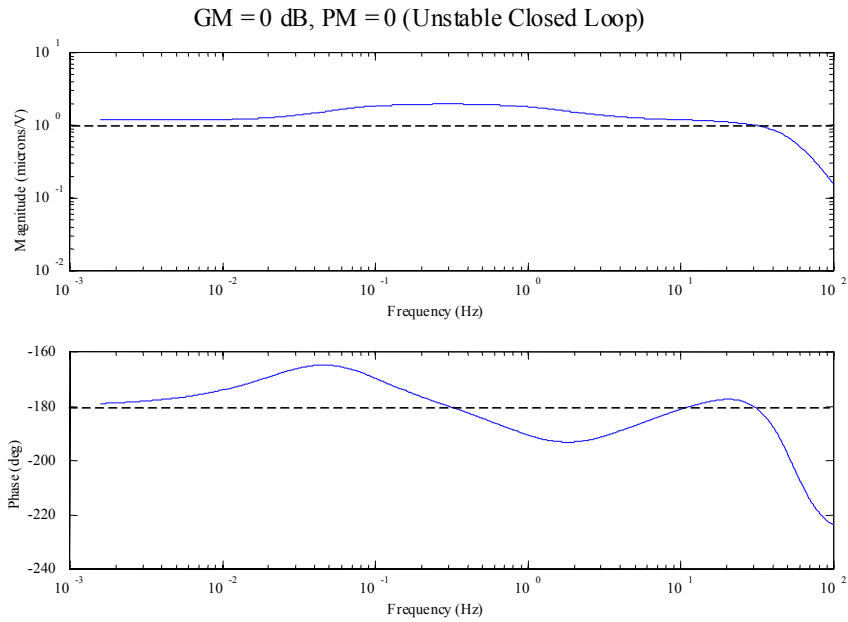


Figure 4.19: Bode plot of the series plant and compensator of the long polymer for a perturbation factor of 9% in Case 2.

to the increase in gain margin of the compensator after the resonant frequency, which adds up to the resonance phenomenon of the plant. Figure 4.21 shows that system for case 2, where $Q = C'_m C_m$ goes unstable at $\Delta = 0.08$.

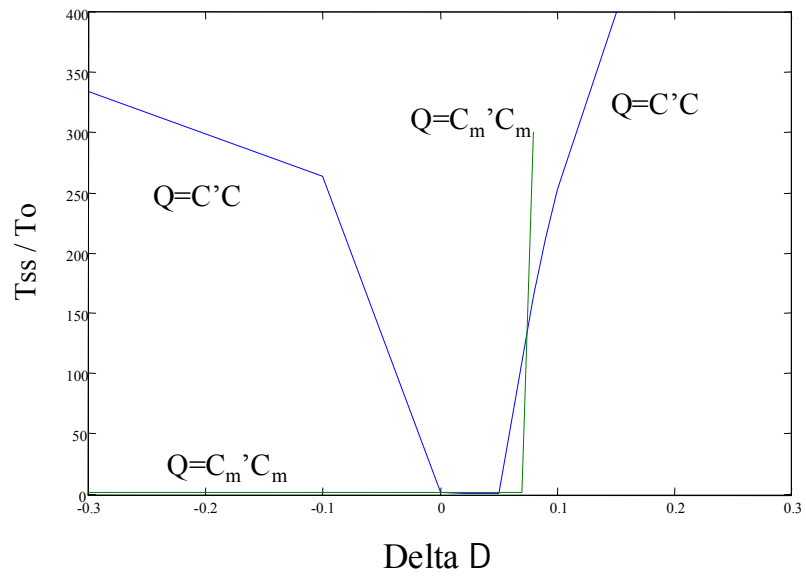


Figure 4.20: Variation of the Settling Time ratio as Perturbation changes ($-0.3 < \Delta < 0.3$).

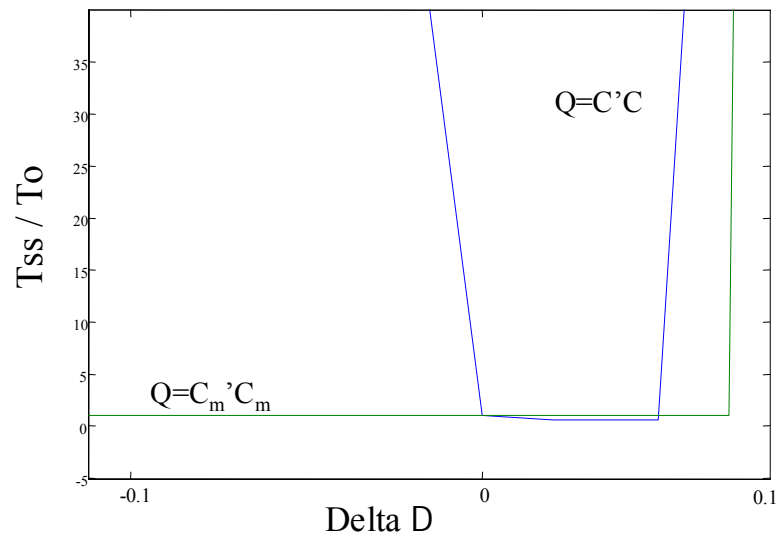


Figure 4.21: Variation of the Settling Time ratio as Perturbation changes ($-0.1 < \Delta < 0.1$).

4.4 Summary

In this chapter, the empirical model developed in the previous chapter was converted into a canonical state space model. The ionic polymer actuator was modeled as a parallel interconnection of subsystems representing single time constants and resonance. A perturbation factor was introduced in the state space model to study the effects of change in resonant frequency on the design of the compensator.

The controller was designed using an observer estimator with LQR techniques. The number of design variables was reduced to one using the LQR method selecting appropriate cost functions. Two cost functions were used which varied in the inclusion of resonance terms. Simulations of the closed-loop system of the short-polymer showed a fast settling time and a high initial control input followed by a slow increase. The stability of the system was discussed using bode plots and the placement of poles was explained using the root locus plot. Simulations of the closed-loop system of the long polymer using cost function *including* the resonance terms showed a fast settling time. Simulations of the closed-loop system of the long polymer using cost function *without including* the resonance terms showed no substantial change in the settling time. The system was close to instability which was illustrated using bode plots and placement of poles using the root locus plot.

To study the effects of change in resonant frequency on the design of the compensator using two different cost functions, simulations of the closed-loop system of the long polymer were performed by varying the perturbation factor from -0.9 to $+0.9$. The design of the compensator using cost function including the resonance terms was more robust compared to the design of the compensator using the cost function which excludes the resonance terms.

The feedback control of the ionic polymer actuator when simulated showed that the settling time is faster when a step input is given. Using the controller, the bandwidth of the actuators can be increased and it can be used to actuate high frequency signals.

Chapter 5

Experimental Analysis

5.1 Experimental setup

In order to experimentally test the feedback controller designed in the previous chapter a test setup was built to perform closed-loop control experiments. Two different sizes of the ionic polymer actuator were used in these set of experiments, summarised in Table 5.1.

Table 5.1: Actuator Samples and their Sizes

Actuator Label	Total Length (mm)	Width (mm)	Thickness (mm)	Unsupported Length (mm)
Short	12	5	0.2	7.8
Long	40	5	0.2	26.3

The closed-loop control experiments are performed on the test setup as shown in Figure 5.1. The schematic test setup shown in Figure 5.2 consists of a set of two electrodes placed at the fixed end of the actuator. The sample is cantilevered from the electrodes. The displacement at approximately the tip of the actuator is measured with a laser vibrometer. The actuator is excited by a voltage supplied by a power amplifier (50 V, 1.2 A) that is controlled by the signal from a digital signal processor (dSPACE, Inc. Model 1102). The digital signal processor also measures the actuator displacement at the tip, the voltage across the actuator, and the current through the actuator. Control algorithms are implemented on the digital signal processor sampling at a rate of $f_s = 1000$ Hz. The voltage levels are limited between -3 Volts to 3 Volts. The sampling rate is deemed large enough so that the controller is designed using continuous time techniques and transformed into a discrete

compensator using a Tustin transformation. Also, the limited frequency content of the input signal (i.e. the step excitation) is such that no anti-aliasing filters are required. In the continuous domain, the state space model of the compensator equations are given in Equation[5.1].

$$\begin{aligned} \hat{\dot{x}}(t) &= (A - BG - KC)\hat{x}(t) + \begin{bmatrix} BG - BG_r & K \end{bmatrix} \begin{Bmatrix} x_r(t) \\ y(t) \end{Bmatrix} \\ u(t) &= -G\hat{x}(t) + \begin{bmatrix} G - G_r & 0 \end{bmatrix} \begin{Bmatrix} x_r(t) \\ y(t) \end{Bmatrix} \end{aligned} \quad (5.1)$$

The continuous state space model is converted into a discretised model by Convert to discrete time using the bilinear (Tustin) approximation to the derivative using the C2DM function provided in MATLAB. In the Tustin method, the continuous s-domain is mapped on to the discretized z-domain using the transformation shown in Equation[5.2].

$$s \leftarrow 2f_s \frac{z - 1}{z + 1} \quad (5.2)$$

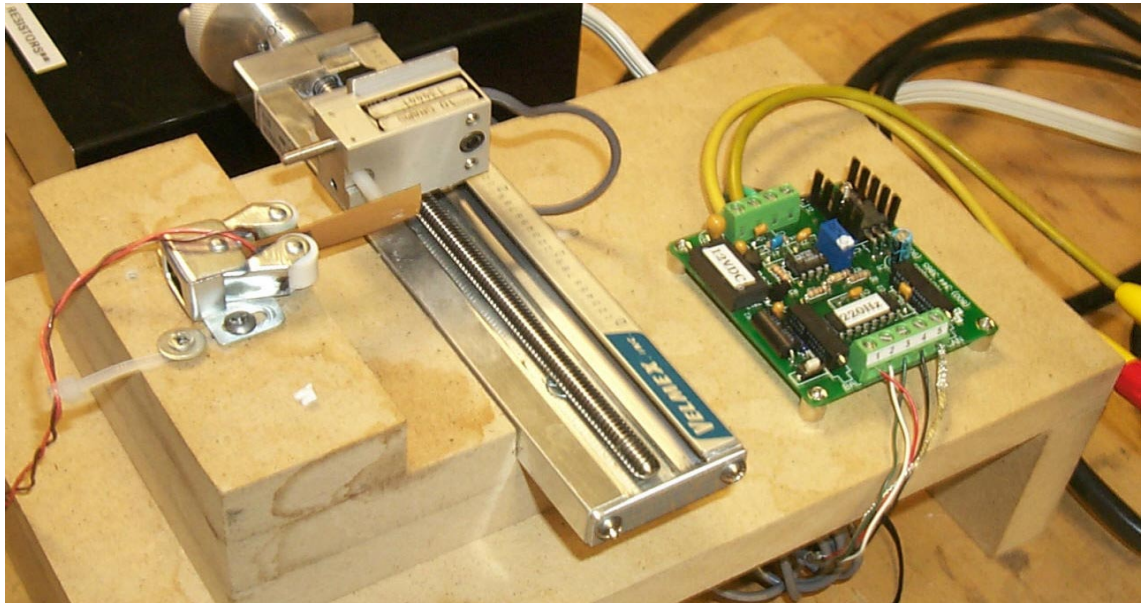


Figure 5.1: Experimental setup for closed-loop control

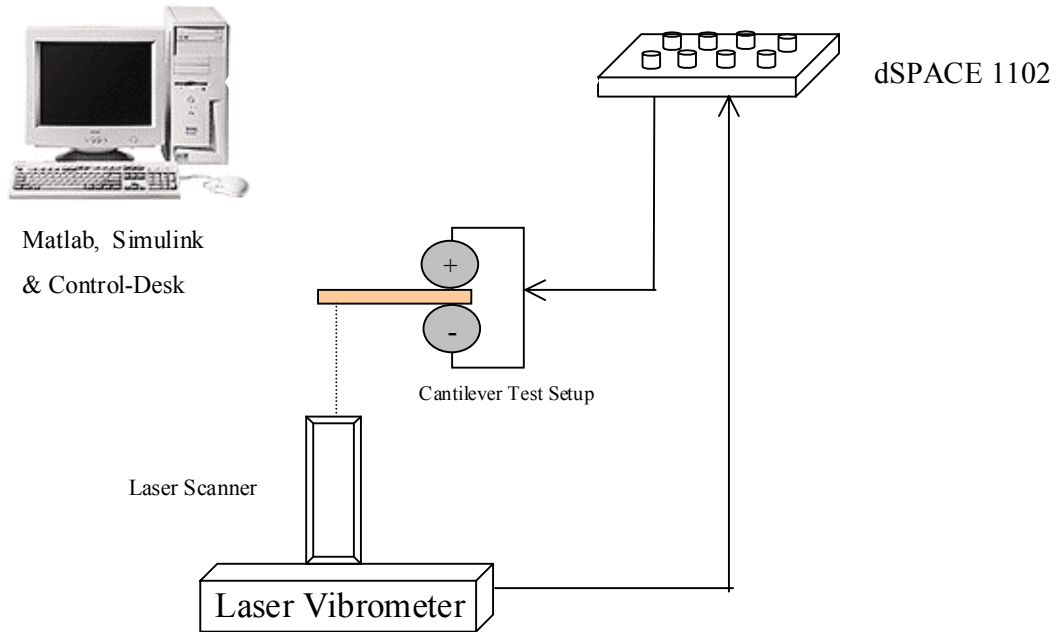


Figure 5.2: Schematic of the experimental setup for closed-loop control

5.2 Experimental Results

5.2.1 Short Polymer

A plot of the tip deflection as a function of time for the shorter polymer in an open-loop and closed-loop is shown in Figure 5.3. The plots have been normalized by their steady-state value to emphasize the difference in settling time and overshoot. The steady-state value for the plot is on the order of $150 \mu\text{m}$ and can be varied by changing the value of the step input to the control system. As predicted by the simulations, feedback control reduces the overshoot and settling time of the tip deflection. The overshoot of the response is reduced from 500% (5:1) to approximately 30% (1.3:1). The settling time is reduced from approximately 13 seconds to between 3 and 4 seconds.

Experimental measurements of the tip displacement, as the values of the gain applied practically are varied, is shown in Figure 5.4. It is observed that as the value of the control design parameter r increased, the settling time is faster.

It is observed that as the value of the control design parameter r increased beyond $r = 10^{-3}$, the system became unstable. As r increases beyond a certain value, the initial control input becomes very high. The system is more sensitive to this sudden spike in the

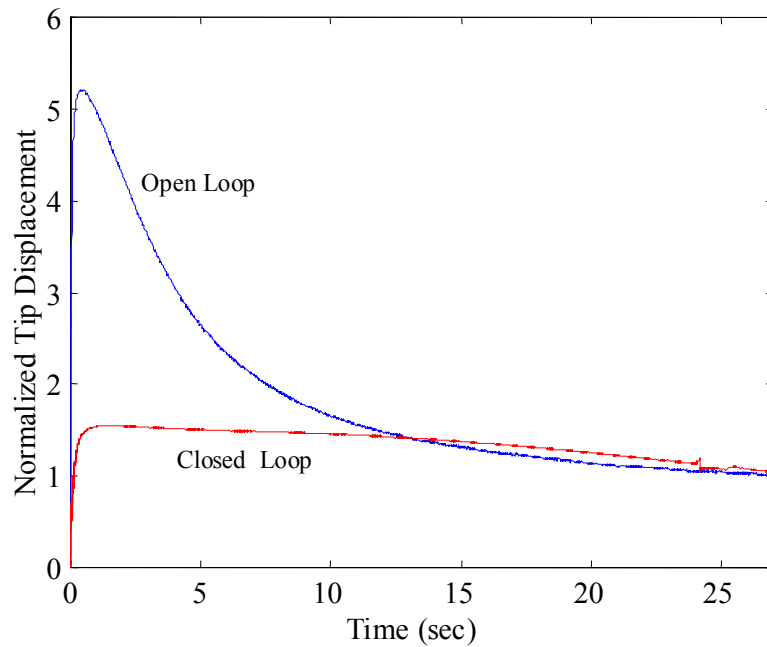


Figure 5.3: Experimental step response for the short polymer in an open-loop and closed-loop.

control input, and causes the ionic polymer actuator to go unstable. Figure 5.5 shows the normalized tip displacement for $r = 10^{-2}$ when a step input of 1 Volt is given. The ionic polymer actuator system becomes unstable within a short period of time on the order of 0.3 seconds. Hence we were limited on the values of the applied gain.

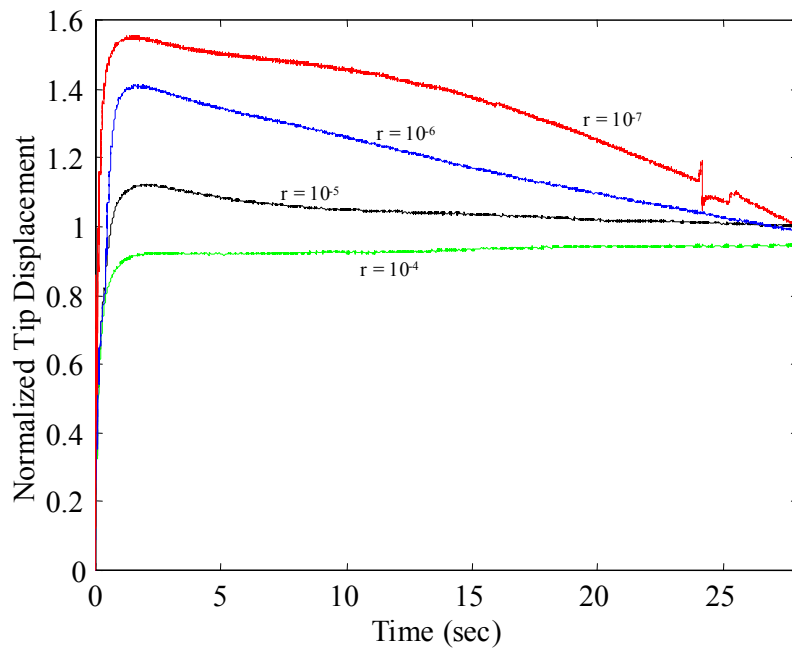


Figure 5.4: Experimental step response for the short polymer in closed-loop for various gains.

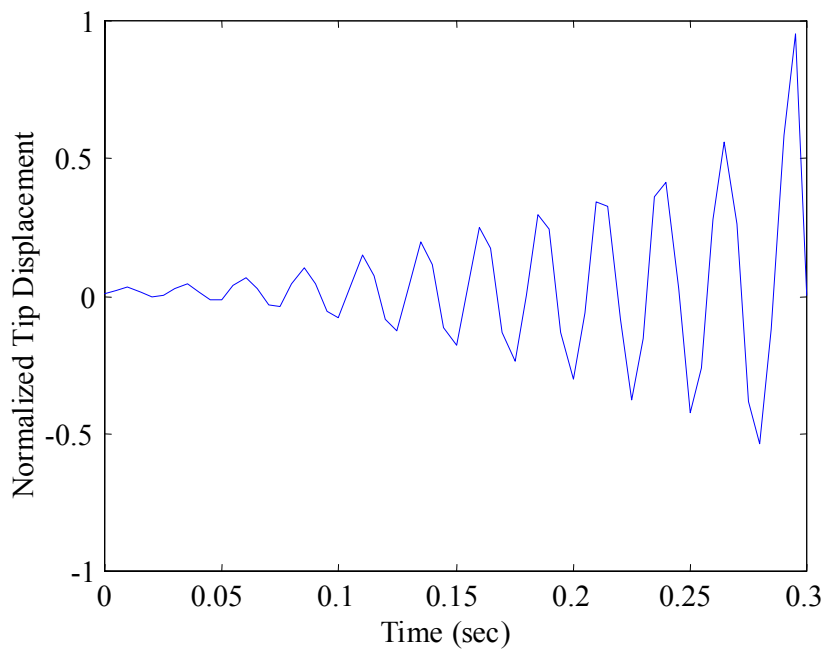


Figure 5.5: Experimental step response for the short polymer in unstable closed-loop at high gain.

5.2.2 Long Polymer

Case 1: Resonance term included in Cost Function

Experimental results for the control of the polymer using the cost function which includes the resonance terms, $Q = C'C$ is shown in the Figure 5.6. It is observed that the settling time is reduced to 3 to 4 seconds when compared to an open-loop settling time of 20 seconds. The plots have been normalized by their steady-state value. The steady-state value for the plot is on the order of $1000 \mu\text{m}$ and can be varied by changing the value of the step input to the control system. As predicted by the simulations, feedback control reduces the overshoot and settling time of the tip deflection. The overshoot of the response is reduced from 1800%(18:1) to approximately 300% (3:1).

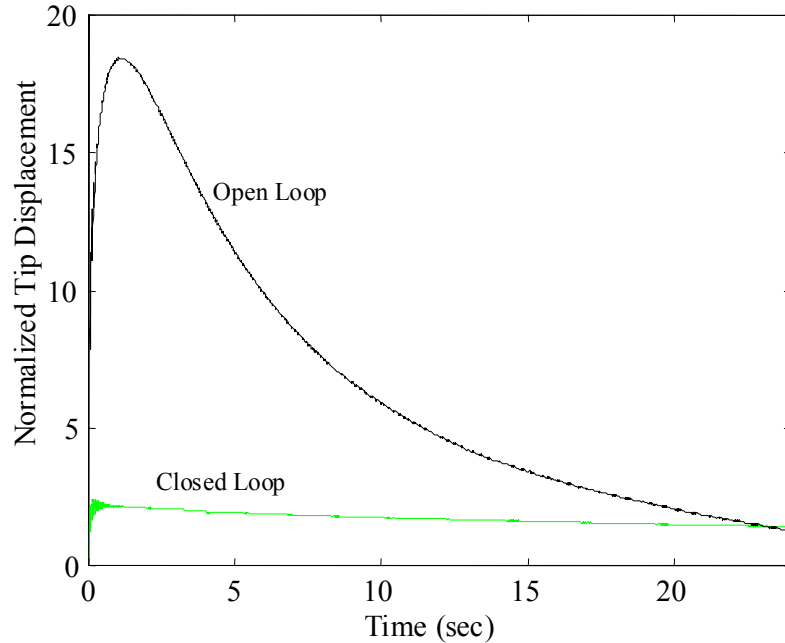


Figure 5.6: Experimental step response for the long polymer in an open-loop and closed-loop.

As r increases, the settling time is faster, but the system is more sensitive to small variations in the resonance of the polymer. Hence we were limited on the values of the applied gain due to changes in the resonant frequency of the actuator. Experimental results of the tip displacement, as the values of the applied gain are varied, is shown in Figure 5.7. The practical gains were limited to $1/3$ and $1/2$ at higher value of r .

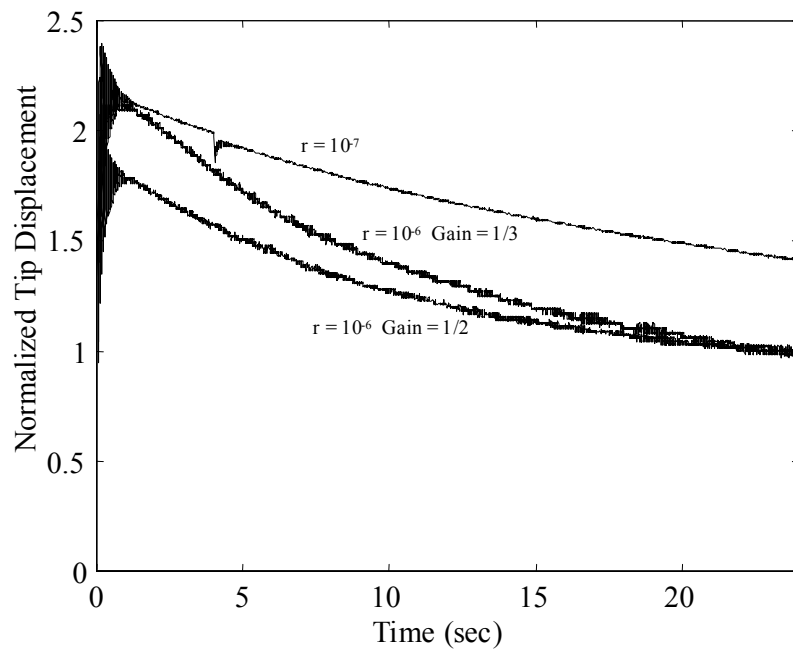


Figure 5.7: Experimental step response for the long polymer in closed-loop for various gains.

Case 2: Resonance terms not included in Cost Function

Experimental results for the control of the polymer using the cost function which does not include the resonance terms, $Q = C_m' C_m$ is shown in the Figure 5.8. It is observed that the settling time is reduced to 4 to 5 seconds when compared to an open-loop settling time of 25 seconds. The plots have been normalized by their steady-state value. The response for the case $Q = C_m' C_m$ achieves a steady-state value near approximately zero tip displacement. This is caused by the fact that the value of r for this form of the state weighting matrix cannot be increased much beyond 10^{-7} due to a closed-loop instability. Any change in the resonance frequency introduces increases in the magnitude of the system frequency response and has the potential to cause instability in the closed loop. Figure 5.9 shows one measurement of the tip displacement at higher gains where the system oscillates and becomes unstable.

As predicted by the simulations, feedback control reduces the overshoot and settling time of the tip deflection. The overshoot of the response is reduced from 1800%(18:1) to approximately 800% (8:1).

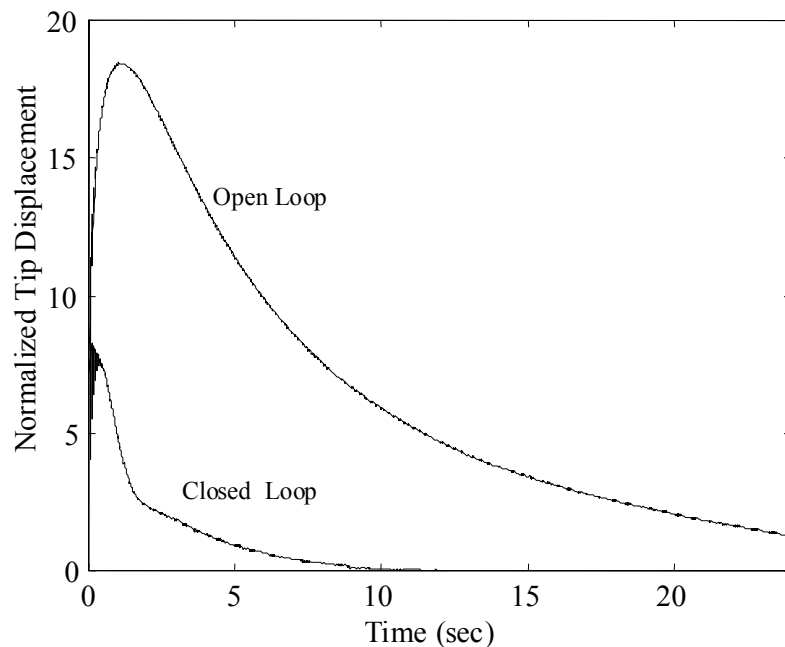


Figure 5.8: Experimental step response for the long polymer in an open-loop and closed-loop.

Experimental results of the tip displacement, as the values of the applied gain are

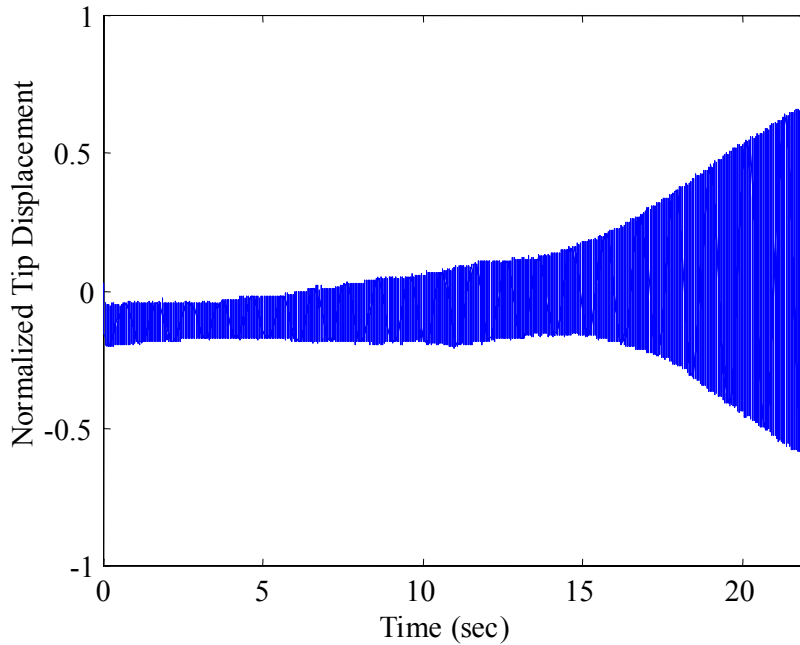


Figure 5.9: Unstable experimental step response for the long polymer in closed-loop for high gain.

varied, is shown in Figure 5.10. The practical gains were as low as $1/20$ and $1/12$ at higher value of r .

5.2.3 Analysis of Results

Experimental results for the short polymer illustrate that feedback control reduces the overshoot and the settling time. By varying the magnitude of the step input, the steady state value can be changed. For high values of the design parameter r , the closed-loop system goes unstable. The experiments follow the simulations to a large extent and satisfactory results are achieved by using feedback control for the short polymer when a step voltage is given.

Experimental results for the control of the long polymer indicate that as the value of the control design parameter r increased, the system became unstable. Although both control systems are limited in their performance, the control system that utilizes the resonant states in the weighting function (Case 1) results in much better performance than the design that ignores the resonant states (Case 2). The response of the ionic polymer actuator (tip displacement) for $Q = C'_m C_m$ has a settling time of 6 seconds, and $Q = C' C$ has a

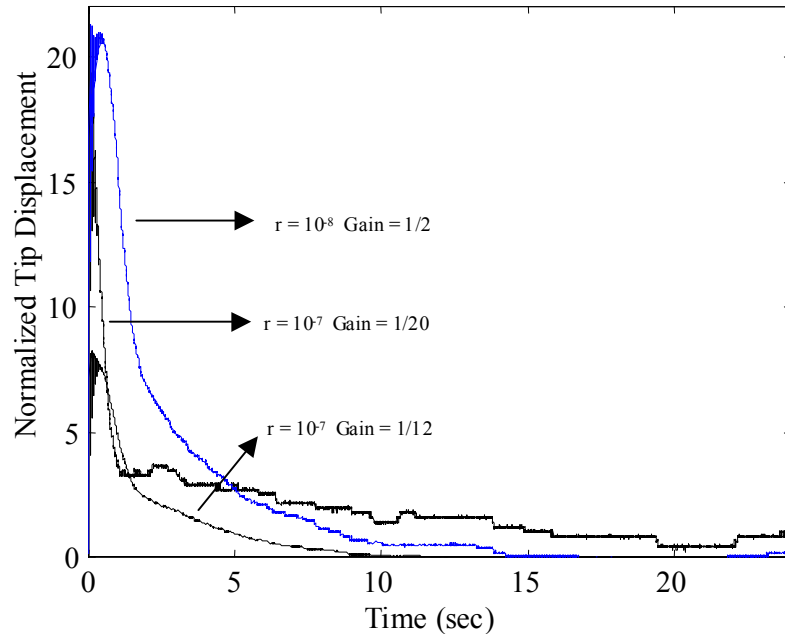


Figure 5.10: Experimental step response for the long polymer in closed-loop for various gains.

settling time of 10 seconds as compared to the open loop settling time of 20 seconds. The simulation shows a much faster response, but due to the limitation of the gains, the experimental response does not match the simulation. An important attribute of the closed-loop response is that the overshoot due to a step is decreased dramatically. We note that the controlled response has an overshoot on the order of 20-30%, compared to the ratio of the peak to steady-state value exhibited by the open-loop response.

For Case 2, the instability is attributed to test-to-test variations in the resonance frequency and the fact that this controller is placing a notch at the resonance frequency of the model. As shown in Figure 4.13b, ideal pole-zero cancellation eliminates the changes in magnitude associated with the actuator resonance and enables the system to have small phase margins and still maintain stability. In contrast, in Case 1, the control design that utilizes $Q = C'C$ places lead compensation in the network to provide additional phase margin near resonance. Additional phase is a more robust method of controlling the resonance because it is less sensitive to small variations in the natural frequency as a result of surface dehydration or test-to-test variations in the resonance.

5.3 Summary

In this chapter, the feedback controller developed in the *Chapter 4* is tested experimentally. The control of short polymer showed reduction in settling time and overshoot. The system was stable for low value of design parameter and instability was observed at high value of design parameter due to the initial spike of current.

The control of the longer polymer was achieved by two methods as shown in the simulations in the previous chapter. Both the methods showed a reduction in settling time and overshoot. In the first method, where the resonance terms were included in the cost function, the closed-loop system was relatively stable when compared to the second method at high value of design parameter r .

Chapter 6

Contributions, Conclusions, Recommendations and Future Work

6.1 Contributions

The following is a list of contributions made in this work:

- The step response of the ionic polymer actuator was studied in a cantilever configuration. The importance of control of resonance was stressed by studying the frequency response data of three different sizes of the polymer. The change in the natural frequency as the ionic polymer dehydrated and re-hydrated was quantified.
- An empirical model was developed and generalized for any length of the polymer. Resonance terms were included to model the resonance seen in longer polymers. The accuracy of the empirical model as a function of the number of real poles in the model was studied for a short and long polymers.
- A linear observer-estimator controller was designed using the LQR techniques which reduced the settling time and the overshoot in closed-loop simulations. The response and stability of the closed-loop system for a long ionic polymer actuator was studied for two different cost functions.
- Experiments were conducted on the closed-loop ionic polymer actuator system. Faster

settling time and reduction in overshoot in the tip displacement was observed by using feedback control. The closed-loop system of the ionic polymer actuator became unstable at high values of the design parameter r , as predicted by the simulations, due to the change in resonance frequency as it dehydrates during testing.

6.2 Conclusions

A test setup to measure the tip displacement of the ionic polymer actuator in a cantilever configuration was built. From the analysis and work in this research, the following conclusions are made:

- The tip displacement of an ionic polymer actuator in a cantilever configuration, to a step input of 1 Volt was studied. The dynamic response showed a fast rise time, on the order of 0.05 seconds, and a slow settling time to steady state on the order of 5-15 seconds. High overshoot was also observed due to the ratio between the peak response and the steady state value.
- The dynamic response for longer polymers was studied. For a step input of 1 Volt, oscillations due to resonance were observed during the first few seconds of the step input. The variation in the stiffness of the actuators due to changes in hydration was studied. The value of the change in the natural frequency mentioned does not represent the entire population of samples tested since a statistical analysis was not presented. For the five experiments performed in the dehydration test, a change of 12.5% in the natural frequency on the first resonance was observed which was caused due to the effect of dehydration and continual usage. For the two experiments performed in the re-hydration test, a change of 6.6% in the natural frequency was observed which did not match with our hypothesis that the natural frequency of the actuator will remain the same if the material is rehydrated after a period of continual use.
- The frequency response data for the 3 different lengths of ionic polymer actuators demonstrate that control of resonance should be given more importance as the length of the polymer increases. Difficulties in controlling the hydration and the change of hydrations as time progresses result in mechanical inconsistency. This necessitates

feedback control to improve and shape the dynamic response of the actuator and increase the bandwidth of the actuator.

- The modeling of the ionic polymer actuator to develop a control model using physical phenomenon is infeasible due to complexities involved and incomplete models suggested. An empirical model suggested by Kanno et al. (1994) was modified to incorporate resonance observed in long polymers and optimized using the least square method. The simulation of such an empirical model to a step input closely matched the experimental data obtained.
- The accuracy of the empirical model as a function of the number of real poles in the model was studied for both short and long polymers. It was observed that increasing the number of real poles did not substantially increase the accuracy of the model. A pole-zero cancellation appeared during the optimization routine if the number of real poles was increased.
- A linear observer estimator was designed using the LQR techniques. The simulations of the closed-loop ionic polymer actuator showed faster settling time and reduction in overshoot.
- The response and stability of the closed-loop system for a long ionic polymer actuator was studied for two different cost functions. The system was more stable for a compensator designed using the cost function which included resonance terms when compared to the system designed using the cost function without the resonance terms.
- Finally, from the experiments, faster settling time and reduction in overshoot in the tip displacement was observed by using feedback control. The overshoot was reduced to 30% in a closed-loop system from an open-loop overshoot in excess of 800%. The settling time was reduced to 4-10 seconds from an open-loop settling time of 20-25 seconds. The closed-loop system of the ionic polymer actuator goes unstable at high values of the design parameter r , as predicted by the simulations, due to the change in resonance frequency as it is dehydrated during testing.

6.3 Recommendations and Future Work

From the experience of this research, the following recommendations on future work are suggested:

- In order to minimize the inconsistency observed in the ionic polymer actuators, it is recommended that the polymers are hydrated for a period of 30 minutes in boiling water. This ensures constant hydration levels during tests and it was observed that the actuators do not dry quickly. It is also recommended that input voltages beyond 3 Volts is not supplied since the polymers undergo electrolysis at the anode.
- To avoid dehydration of water in the ionic polymer actuators, future work on the development of techniques to encapsulate is recommended. This will allow the ionic polymer actuator to be tested for longer times and better consistency can be obtained.
- Various methods of preparation of the ionic polymer actuators with various metals such as nickel, titanium and silver to obtain low surface resistance need to be developed.
- Physical models and characteristics of the ionic polymer actuators and sensors have to be developed. Such models can be used directly by systems and control researchers. The relationship between the blocked force output as the voltage changes need to be studied to develop more practical applications.
- For practical applications, the response of the ionic polymer actuator to a S-curve input, square input and sinusoidal inputs should be studied. A controller can be designed using the techniques used in this work for the same.
- The design of a compensator for the single-input single-output can be further developed into a multi-input multi-output system. The compensator can also be designed to handle inputs which give a reference value of a force or a tip deflection instead of a voltage.
- The tip displacement which was measured using a laser vibrometer needs to be measured more accurately. Sensors like PZTs or another ionic polymer may be attached to the end of the actuator and used for the tip displacement after calibration.

- Other configurations, such as a fixed-fixed configuration of the ionic polymer actuator can be studied.
- The cost function used for the optimization can be further improved by giving weights to the resonance data to model them more accurately
- The empirical model developed in this work can include more resonance terms to accurately model the dynamics of the long polymer

Bibliography

Bennett, M., 2001, "Preparation of electroactive polymers at CIMSS, Virginia Tech," Personal communication.

Cohen, Y., T.Xue, Shahinpoor, M., J.O.Simpson, and J.Smith, *Flexible, Low-Mass Robotic Arm Actuated by Electroactive Polymer*, **Proceedings of the SPIE Conference**, Vol. 3329, pp. 52–57, 1998.

Coleman, T. F. and Zhang, Y., 2000, **Optimization Toolbox - For Use with MATLAB**, The Mathworks, Inc., 3 Apple Hill Drive, Natick, MA 01760-2098, 2nd edn.

de Gennes, P., Shahinpoor, M., and Kim, K., *Mechanoelectric Effect in Ionic Gels*, **Europhysics Letters**, 1999.

Friedland, B., **Control System Design, An Introduction to State Space Methods**, McGraw-Hill, Inc., New York, New York, 1986.

Guo, S., Fukuda, T., Kato, N., and Oguro, K., *Development of a Underwater Microrobot using ICPF Actuator*, **Proceedings of the IEEE International Conference on Robotics and Automation**, pp. 1829–1834, 1998.

Guo, S., Fukuda, T., Nakamura, T., Aria, F., Oguro, K., and Negoro, M., *Micro Active Guide Catheter System Characteristic Evaluation, Electrical Model and Operability Evaluation of Micro Active Catheter*, **Proceedings of the IEEE International Conference on Robotics & Automation**, pp. 2226–2231, 1996.

Guo, S., Hata, S., Sugumoto, K., Fukuda, T., and Oguro, K., *Development of a New Type of Capsule Micropump*, **Proceedings of the IEEE International Conference on Robotics & Automation**, pp. 2171–2176, 1999.

Guo, S., Nakamura, T., Fukuda, T., and Oguro, K., *Development of a Micropump using ICPF Actuator*, **Proceedings of the IEEE International Conference on Robotics and Automation**, pp. 1829–1834, 1997.

Hunter, I. and Lafontaine, S., *A Comparison of Muscle with Artificial Actuators*, **Technical Digest of the IEEE Solid-State Sensor and Actuator Workshop, Hilton Head, South Carolina**, pp. 178–185, 1992.

Kanno, R., Kurata, A., Hattori, M., Tadokoro, S., and Takamori, T., *Characteristics and Modeling of ICPF Actuator*, **Proceedings of the Japan-USA Symposium on Flexible Automation**, Vol. 2, pp. 691–698, 1994.

Kanno, R., Tadokoro, S., and Takamori, T., *3-Dimensional Dynamic Model of Ionic Conducting Polymer Gel Film (ICPF) Actuator*, **Proceedings of the IEEE International Conference on Robotics and Automation**, pp. 2179–2184, 1996a.

Kanno, R., Tadokoro, S., Takamori, T., and Hattori, M., *Linear Approximate Dynamic Model of ICPF (Ionic Conducting Polymer Gel Film) Actuator*, **Proceedings of the IEEE International Conference on Robotics and Automation**, Vol. 1, pp. 219–225, 1996b.

Karim Salehpoor, M. S. and Mojarrad, M., *Linear and Platform Type Robotic Actuators made from Ion Exchange Membrane Metal Composites*, **Proceedings of the SPIE Conference**, Vol. 3040, pp. 192–198, 1997.

Lawrance, R. and Wood, L. D., *Method of making Solid Polymer electrolyte Catalytic Electrodes*, **United States Patent 4,272,353**, 1980.

Liu, R., Her, W., and Fedkiw, P. S., *In Situ Electrode Formation on a Nafion Membrane by Chemical Platinization*, **Journal of Electrochemical Society**, Vol. 139, No. 1, pp. 15–23, 1992.

Mallavarapu, K., Newbury, K., and Leo, D., *Feedback Control of the bending Response of Ionic Polymer Metal Composite Actuators*, **Proceedings of the SPIE March 4-8 Conference, Newport Beach, CA**, 2001.

Mojarrad, M. and Shahinpoor, M., *Noiseless Propulsion for Swimming Robotic Structures Using Polyelectrolyte Ion-Exchange Membranes*, **Proceedings of the SPIE Conference**, Vol. 2716, No. 27, pp. 183–192, 1996.

Mojarrad, M. and Shahinpoor, M., *Ion Exchange Metal Composite Sensor Films*, **Proceedings of SPIE**, Vol. 3042, pp. 52–60, 1997.

Mojarrad, M., Shahinpoor, M., and Salehpoor, K., *Electrically Induced Large Amplitude Vibration and Resonance Characteristics of Ionic Polymeric Membrane-Metal Composites Artificial Muscles*, **Proceedings of SPIE Msrat Material & Structures Conference**, Vol. 3041, No. 76, pp. 829–838, 1997.

Nemat-Nasser, S. and Li, J. Y., *Electromechanical Response of Ionic Polymer Metal Composites*, **Proceedings of the SPIE Conference**, Vol. 3987, pp. 82–91, 2000.

Newbury, K. and Leo, D., *Mechanical Work and Electromechanical Coupling in Ionic Polymer Bender Actuators*, **Proceedings of the IMECE Nov 11-16, New York, NY**, 2001, To be published.

Oguro, K., Fujiwara, N., Asaka, K., Onishi, K., and Sewa, S., *Polymer Electrolyte Actuator with Gold Electrodes*, **Proceedings of the SPIE Conference**, Vol. 3669, pp. 64–71, 1999.

Shahinpoor, M., *Nonhomogeneous Large Deformation theory of Ionic Polymeric Gels in Electric and pH Fields*, **Proceedings of SPIE Conference on Smart Structures and Materials**, Vol. 1916, pp. 40–50, 1993.

Shahinpoor, M., *Design and Modeling of a Novel-Spring Loaded Ionic Polymer Gel Actuator*, **Proceedings of SPIE North American Conference on Smart Structures and Materials**, Vol. 2189, No. 26, pp. 255–264, 1994a.

Shahinpoor, M., *Microelectro-Mechanics of Ionic Polymeric Gels As Synthetic Robotic Muscles*, **Proceedings of SPIE North American Conference on Smart Structures and Materials**, Vol. 2189, No. 27, pp. 265–274, 1994b.

Shahinpoor, M., *Active Polyelectrolyte Gels as Electrically Controllable Artificial Muscles and Intelligent Network Structures*, **Structronic Systems: Smart Structures, devices and Systems, Part II: Systems and Controls**, World Scientific, pp. 31–85, 1998.

Shahinpoor, M., *Electro-mechanics of Iono-Eleactic Beams as Electrically-Controllable Artificial Muscles*, **Proceedings of SPIE Conferences on Electroactive Polymer Actuators and Devices**, Vol. 3669, pp. 109–121, 1999.

Shahinpoor, M., Cohen, Y., J.O.Simpson, and J.Smith, *Ionic Polymer-Metal Composites (IPMC) as Biomimetic Sensors, Actuators and Artificial Muscles - A Review*, **International Journal of Smart Materials and Structures**, Vol. 7, pp. R15–R30, 1998.

Shahinpoor, M., Mojarrad, M., and Salehpoor, K., *Electrically-Induced Large Amplitude Vibration and Resonance Characteristics of Ionic Polymeric Membrane- Metal Composites*, **Proceedings of SPIE Smart Materials and Structures Conference**, Vol. 3041, No. 76, pp. 829–838, 1997.

Tadokoro, S., Murakami, T., Fuji, S., Kanno, R., Hattori, M., and Takamori, T., *An Elliptic Friction Drive Element Using an ICPF Actuator*, **IEEE Control Systems**, Vol. 17, No. 3, pp. 60–68, 1997.

Tadokoro, S., Yamagami, S., Ozawa, M., Kimura, T., and Takamori, T., *Multi-DOF Device for Soft Micromanipulation Consisting of Soft Gel Actuator Elements*, **Proceedings of the IEEE International Conference on Robotics & Automation**, pp. 2177–2182, 1999.

Tadokoro, S., Yamagami, S., Takamori, T., and Oguro, K., *Modeling of Nafion-Pt Composite Actuators (ICPF) by Ionic Motion*, **Proceedings of SPIE, Smart Structures and Materials**, Vol. 3987, pp. 92–102, 2000.

Takenaka, H., Torikai, E., Kawami, Y., and Wakabayashi, N., *Solid Polymer Electrolyte Water Electrolysis*, **International Journal of Hydrogen Energy**, Vol. 7, No. 5, pp. 397–403, 1982.

Wax, S. and Sands, R., *Electroactive Polymer Actuators and Devices*, **Proceedings of the SPIE Conference on Electroactive Polymers**, Vol. 3669, No. 2, pp. 2–9, 1999.

Yanjing, L., Zeng, T., Y.W., W., and H., Y., *Self Assembled Flexible Electrodes on Electroactive Polymer Actuators*, **Proceedings of the SPIE Conference**, Vol. 3669, pp. 284–288, 1999.

Vita

Kiran Mallavarapu, son of Mallavarapu Adinarayana Murthy and Pulley Vijayalakshmi, was born on September 16, 1978, in Bapatla, India. He was raised in Bangalore. He graduated from Kendriya Vidyalaya, Indian Institute of Science, Bangalore in May 1995. He enrolled in M.S.Ramaiah Institute of Technology, Bangalore University later that August, and graduated in December 1999 with a Bachelor of Engineering in Mechanical Engineering. He enrolled at Virginia Tech to pursue a Master of Science in Mechanical Engineering with the Center for Intelligent Material Systems and Structures (CIMSS), concentrating on Ionic Polymer Actuator and Controls.

Permanent Address: C-408, Quarters
Indian Institute of Science,
Bangalore, Karnataka
INDIA

This thesis was typeset with L^AT_EX 2_ε¹ by the author.

¹L^AT_EX 2_ε is an extension of L^AT_EX. L^AT_EX is a collection of macros for T_EX. T_EX is a trademark of the American Mathematical Society. The macros used in formatting this thesis were written by Greg Walker, Department of Mechanical Engineering, Virginia Tech.